Mitigation of NADPH Oxidase 2 Activity as a Strategy to Inhibit Peroxynitrite Formation*⁣[S]

Jacek Zielonka[‡1], Monika Zielonka[‡], Lynn VerPlank[§], Gang Cheng[‡], Micael Hardy[¶], Olivier Ouari[¶],
Mehmet Menaf Ayhan[¶], Radosław Podsiadły[‡2], Adam Sikora[‖], J. David Lambeth[**], and Balaraman Kalyanaraman[‡3]

From the [‡]Department of Biophysics and Free Radical Research Center, Medical College of Wisconsin, Milwaukee, Wisconsin
53226, [§]Broad Institute of MIT and Harvard, Cambridge, Massachusetts 02142, the [¶]Aix-Marseille Université, CNRS, ICR UMR 7273,
13397 Marseille, France, the [‖]Institute of Applied Radiation Chemistry, Faculty of Chemistry, Lodz University of Technology,
Żeromskiego 116, 90-924 Lodz, Poland, and the [**]Department of Pathology and Laboratory Medicine, Emory University,
Atlanta, Georgia 30322

Using high throughput screening-compatible assays for superoxide and hydrogen peroxide, we identified potential inhibitors of the NADPH oxidase (Nox2) isoform from a small library of bioactive compounds. By using multiple probes (hydroethidine, hydropropidine, Amplex Red, and coumarin boronate) with well defined redox chemistry that form highly diagnostic marker products upon reaction with superoxide (O_2^-), hydrogen peroxide (H_2O_2), and peroxynitrite ($ONOO^-$), the number of false positives was greatly decreased. Selected hits for Nox2 were further screened for their ability to inhibit $ONOO^-$ formation in activated macrophages. A new diagnostic marker product for $ONOO^-$ is reported. We conclude that the newly developed high throughput screening/reactive oxygen species assays could also be used to identify potential inhibitors of $ONOO^-$ formed from Nox2-derived O_2^- and nitric oxide synthase-derived nitric oxide.

NADPH oxidase (Nox)[4] enzymes (Nox1–5 and Duox1/2) have been proposed as potential therapeutic targets in the treatment of a variety of inflammatory and fibrotic diseases, including cancer (1–3). Unlike other redox-active enzymes for which

generation of reactive oxygen species (ROS) is an "accidental" by-product of their primary catalytic function, the only known function of Nox enzymes is generation of ROS (e.g. O_2^- and H_2O_2) (Fig. 1) (4, 5). Several Nox isoforms, including Nox2, form both O_2^- and H_2O_2 (via dismutation of O_2^-), with the exception of Nox4, which generates primarily H_2O_2 with little or no detectable O_2^- (4, 5). A major impediment to advancing Nox research is the paucity of selective inhibitors of Nox isoforms, including Nox1 and -2 (6). This is due in part to the lack of reliable and high throughput-compatible detection probes and assays that are specific for O_2^- and H_2O_2. With the recent discovery of new probes with well defined redox chemistry that form highly diagnostic marker products upon reaction with ROS/RNS both under *in vitro* and *in vivo* conditions and high throughput global profiling assays (Table 1) (7), we can now screen a small library of bioactive compounds. One of the objectives of this study is to identify small molecule inhibitors of the Nox2 isoform using the high throughput screening (HTS)/ROS-based assay(s) that largely eliminate false positives. Previously, we reported the power of our newly developed HTS/ROS assays in identifying true "hits" for Nox2 inhibition and eliminating false positives at the outset (8). Typically, the chemiluminescent probe, L-012, has been used in Nox assay (9). Comparison between L-012 assay and our HTS/ROS assay revealed that L-012 increased false positives by at least a factor of 4 and that this increase is due to inhibition of peroxidase enzyme used in the L-012/Nox assay (10). A related objective of this study is to also identify new small molecule inhibitors of RNS (e.g. peroxynitrite). Peroxynitrite ($ONOO^-$) is a potent oxidizing and nitrating species formed from a diffusion-controlled reaction between O_2^- and nitric oxide ($^\bullet NO$) (Fig. 1) (11, 12) and has been implicated in various neurodegenerative and cardiovascular diseases (13–15). Although ongoing efforts focus on antinitration strategies mostly through direct scavenging of $ONOO^-$ and/or related species (16), a better approach is to suppress the sources of generation of O_2^- (Nox) and/or inhibition of nitric-oxide synthase, particularly inducible NOS (Fig. 1) (17, 18). In this study, we identified several candidate Nox2 inhibitors through HTS-based ROS assays from testing a library of >2,000 bioactive compounds at Broad Institute. Selected hits for Nox2 inhibition were further tested for inhibition of $ONOO^-$ formation in activated macrophages. Results suggest that the HTS/ROS strategy developed herein could be used to

[1] To whom correspondence may be addressed: Dept. of Biophysics, Medical College of Wisconsin, 8701 Watertown Plank Rd., Milwaukee, WI 53226. Tel.: 414-955-4000; Fax: 414- 955-6512; E-mail: jzielonk@mcw.edu.

[2] Present address: Institute of Polymer and Dye Technology, Faculty of Chemistry, Lodz University of Technology, Stefanowskiego 12/16, 90-924 Lodz, Poland.
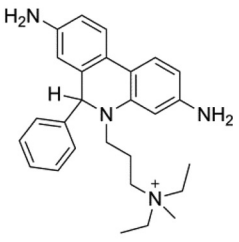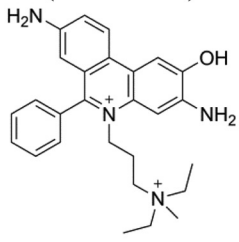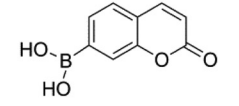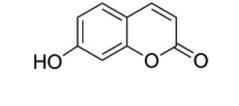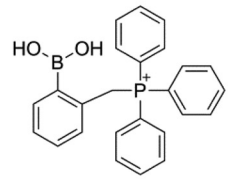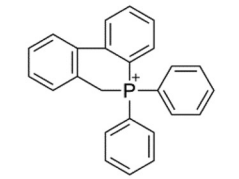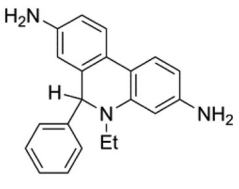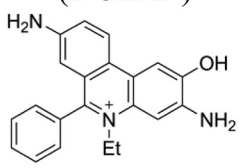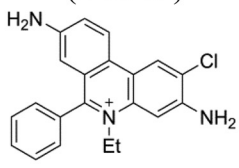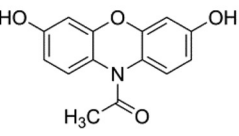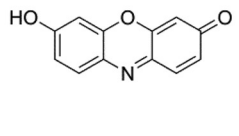
[3] To whom correspondence may be addressed: Dept. of Biophysics, Medical College of Wisconsin, 8701 Watertown Plank Rd., Milwaukee, WI 53226. Tel.: 414-955-4000; Fax: 414- 955-6512; E-mail: balarama@mcw.edu.

[4] The abbreviations used are: Nox, NADPH oxidase; HTS, high throughput screening; ROS, reactive oxygen species; RNS, reactive nitrogen species; HE, hydroethidine; SOD, superoxide dismutase; CBA, coumarin boronic acid; HPr^+, hydropropidine; 2-OH-Pr^{2+}, 2-hydroxypropidium; 2-OH-E^+, 2-hydroxyethidium; PMA, phorbol myristate acetate; cyclo-*o*-MitoPh, 9,10-dihydro-9,9-diphenyl-9-phosphoniaphenanthrene bromide; COH, 7-hydroxycoumarin; *d*HL60, differentiated HL60; MPO, myeloperoxidase; HBSS, Hanks' balanced saline solution; DEPMPO, 5-(diethoxyphosphoryl)-5-methyl-1-pyrroline-*N*-oxide; DPI, diphenyleneiodonium; dtpa, diethylenetriaminepentaacetate.

TABLE 1
Structures of ROS/RNS-specific probes, their reaction products and detection methods

Probe	Diagnostic product(s)	ROS/RNS species	Detection technique(s)
Hydropropidine (HPr$^+$)	2-Hydroxypropidium (2-OH-Pr^{++})	$O_2^{\bullet-}$-specific product	• HPLC with fluorescence detection • LC-MS • Fluorimetry of the complex of 2-OH-Pr^{++} with DNA
Coumarin boronic acid (CBA)	7-Hydroxycoumarin (COH)	H_2O_2 (catalase-sensitive)	• HPLC with fluorescence detection • LC-MS • Fluorimetry
		ONOO$^-$ (catalase-insensitive)	
		HOCl (catalase-sensitive, MPO inhibitor-sensitive)	
ortho-MitoPhB(OH)$_2$	*cyclo-o*-MitoPh	ONOO$^-$-specific product	• LC-MS
Hydroethidine (HE)	2-Hydroxyethidium (2-OH-E$^+$)	$O_2^{\bullet-}$-specific product	• HPLC with fluorescence detection • LC-MS • Fluorimetry of the complex of 2-OH-E$^+$ with DNA
	2-Chloroethidium (2-Cl-E$^+$)	HOCl-specific product	• LC-MS
Amplex Red	Resorufin	H_2O_2 (HRP-dependent, catalase-sensitive)	• HPLC with fluorescence detection • Fluorimetry

FIGURE 1. **Generation of reactive oxygen and reactive nitrogen species from NADPH oxidase and nitric-oxide synthase, and their abrogation by Nox inhibitors and ROS/RNS scavengers.**
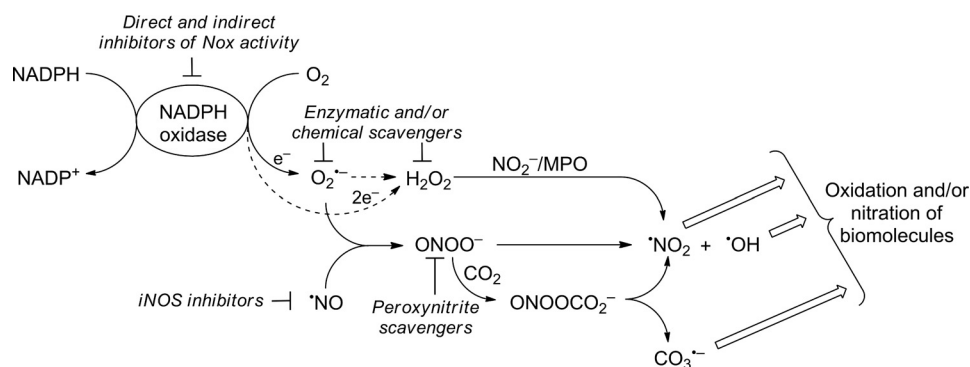
identify Nox2 inhibitors that inhibit $ONOO^-$ formation. In this study we also discovered a new diagnostic marker product for specific detection and quantitation of peroxynitrite in biological systems. One of the objectives of this study is to also use these candidate inhibitors of Nox2 as potential inhibitors of $ONOO^-$ generated via Nox2 intermediacy.

Experimental Procedures

Materials—All compounds in the HTS library were routinely dissolved in DMSO and stored at $-20\ °C$. DMSO concentration ($<1\%$) was kept the same in both control and treatment conditions. In confirmatory studies, stock solutions were prepared at higher concentrations (typically 10 mM or higher), such that the final concentration of the solvent vehicle was kept minimal ($<0.3\%$ v/v) upon dilution. Hydropropidine (HPr^+), coumarin boronic acid (CBA), and *ortho*-mito-phenylboronic acid (o-MitoPhB(OH)$_2$) were synthesized according to published procedures (19–22). Deuterated (d_{15}) analogs of o-MitoPhB(OH)$_2$ and o-MitoPhNO$_2$ were synthesized in the analogous protocol to o-MitoPhB(OH)$_2$ but using deuterated triphenylphosphine (d_{15}-PPh$_3$), whereas d_{15}-o-MitoPhOH was synthesized by oxidation of d_{15}-o-MitoPhB(OH)$_2$ by excess H_2O_2. Amplex Red (10-acetyl-3,7-dihydroxyphenoxazine), resorufin, and 7-hydroxycoumarin were purchased from Cayman and Sigma. Hydroethidine (HE) was from Invitrogen. Authentic standards of 2-hydroxyethidium (2-OH-E^+) and 2-hydroxypropidium (2-OH-Pr^{2+}) were synthesized as described previously (19, 23, 24). Stock solutions of CBA, HE, and Amplex Red were prepared at 20–100 mM concentration in DMSO and stored at $-80\ °C$. For experiments involving HOCl, DMSO was replaced with ethanol. Horseradish peroxidase (HRP, type VI), superoxide dismutase (SOD), catalase and all other reagents were obtained from Sigma.

For organic synthesis, THF was distilled under dry argon atmosphere in the presence of sodium and benzophenone. All reagents were used as received without further purification. The reactions were monitored by TLC on silica gel (Merck 60F254). Crude materials were purified by flash chromatography on Merck silica gel 60 (0.040–0.063 mm). ^{31}P NMR, ^1H NMR, and ^{13}C NMR spectra were recorded with Bruker DPX 300 or 400 spectrometers at 121.49, 300.13, and 75.54 MHz, respectively. ^{31}P NMR measurements were carried out in CDCl$_3$ using 85% H$_3$PO$_4$ as an external standard with broad band ^1H decoupling. ^1H NMR and ^{13}C NMR measurements were carried out in CDCl$_3$ using TMS or CDCl$_3$ as internal reference, respectively. Chemical shifts (δ) are reported in parts/million and coupling constant J values in hertz. Mass spectrometry analyses were performed at the University of Aix-Marseille (Spectropole).

HTS-compatible Cellular Models of Nox2—Human promyelocytic leukemia HL60 cells (Sigma) differentiated into neutrophil-like cells by all-*trans*-retinoic acid were used as the HTS-compatible source of Nox2 model system for screening Nox2 inhibitors (25, 26). HL60 cells were incubated with all-*trans*-retinoic acid (1 μM) for 4–5 days for converting nondifferentiated cells into differentiated cells. Nox2 activation was achieved by treating differentiated HL60 (dHL60) cells with phorbol myristate acetate (PMA, 1 μM) (8).

High Throughput Screening of the Small Library of Bioactive Compounds at Broad Institute—To test the inhibitory effects of the compounds included in the library of the bioactive compounds, we preincubated dHL60 cells with the potential inhibitors for 30 min, followed by addition of PMA and the appropriate probe, as shown in Table 2. After 90 min of incubation at 37 °C in a CO$_2$-free incubator, the extent of oxidation of the probes was measured with PerkinElmer Life Sciences Envision plate reader (PerkinElmer Life Sciences) using the following excitation/emission filter sets: 485/590 nm, 355/460 nm, and 531/595 nm, for hydropropidine + DNA, coumarin boronic acid, and Amplex Red + HRP, respectively.

Signal Optimization, HTS Statistics, and Z′ Values—We used the Z′ factor method as a measure of the assay quality or performance. As positive control (control+ signal), dHL60 cells were incubated with PMA in the presence of DMSO. The negative control (control− signal) included cells in the presence of phenylarsine oxide (1 μM) used as Nox2 inhibitor. The dynamic range was established by the difference between averaged maximal (control+) and minimal (control−) signals. The Z′ factor was calculated using Equation 1 (27),

$$Z' = 1 - \frac{3SD_{control+} + 3SD_{control-}}{|mean_{control+} - mean_{control-}|} \quad (\text{Eq. 1})$$

where control+ and control− correspond to PMA-stimulated cells in the presence of DMSO only or 1 μM phenylarsine oxide, respectively, and S.D. values are the corresponding standard deviations.

Nox2 Inhibition as Anti-nitration Strategy

The calculated Z′ values determined at Broad Institute in 384-well plates for all three HTS assays (hydropropidine + DNA, coumarin boronic acid, and Amplex Red + HRP) were 0.45, 0.64, and 0.79, respectively. Assuming the inhibitor identification threshold of 3× S.D. deviation of the neutral (negative) control (DMSO), we can determine positive hits with a 42, 28, and 15% inhibition for hydropropidine + DNA, coumarin boronic acid, and Amplex Red + HRP, respectively.

Oxygen Consumption Experiments—Nox activity was determined by measuring rates of oxygen consumption in PMA-activated differentiated HL60 cells using a Seahorse XF96 extracellular flux analyzer (8, 28). Cell suspensions were prepared in phenol red-free RPMI 1640 medium (without bicarbonate) and aliquoted (80 μl per well) into 96-well plates to obtain a final cell count of 2×10^4 cells per well. After spinning down the cells, additional RPMI 1640 medium (100 μl per well) was added. Oxygen measurements were initiated, and at the specified time points, inhibitors of Nox were added, followed by injection of PMA. Alternatively, cells were pre-incubated with Nox2 inhibitors and transferred into measurement plates, and the response to PMA was tested. We used rotenone (1 μM) and antimycin (10 μM) to dissect out the contribution of mitochondrial respiration to the total oxygen consumption rate. This also enables one to monitor the effects of Nox2 inhibitors on mitochondrial respiration (8).

Synthesis of 9,10-Dihydro-9,9-diphenyl-9-phosphoniaphenanthrene bromide (cyclo-o-MitoPh)—cyclo-o-MitoPh was obtained by adapting the procedures described in the literature (29–31). The scheme for synthesis of cyclo-o-MitoPh is shown in Fig. 9a. Briefly, after formulation of compound **1** in the presence of n-butyl lithium and N,N-dimethylformamide, compound **2** was reduced by sodium borohydride to obtain compound **3**. Bromation of compound **3** by PBr$_3$ afforded compound **4** (29). A solution of 2′-bromo-2-bromomethylbiphenyl **4** (3.3 g, 10 mmol) in methanol (100 ml) was heated under reflux for 24 h. After solvent removal, the light yellow liquid compound was distilled from the reaction mixture to obtain 2′-bromo-2-methoxymethylbiphenyl **5** (2.5 g, 90%) with the following parameters: ^{1}H NMR (400 MHz): δ 7,66–7.64 (1H, d, J = 8.2), 7.55–7.54 (1H, d, J = 7.2), 7.44–7.40 (1H, t), 7.37–7.34 (2H, m), 7.27–7.21 (2H, m), 7.16–7.14 (1H, d, J = 6.5), 4.29–4.26 (1H, d, J = 12.3), 4.17–4.14 (1H, d, J = 12.3), 3.25 (3H, s); and ^{13}C NMR (300 MHz): δ 141.8–141.4 (d), 140.8–140.2 (d), 136.1 (s), 135.4 (s), 132.5 (s), 131.1 (s), 130.0 (s), 129.6–129.0 (m), 128.1–128.1 (d), 127.9–127-2 (m), 127.1–127.0 (d), 123.6 (s), 72.4–72.0 (d), 58.2–58.1 (d). MS calculated for $C_{14}H_{13}BrO$ was 277.1 and found was 277.1.

The Grignard reagent was prepared from 2′-bromo-2-methoxymethylbiphenyl **5** (1.6 g, 5.8 mmol), magnesium turnings (0.4 g), and trace amount of iodine in THF (20 ml). Then diphenylphosphinous chloride (1.91 g, 8.6 mmol) in THF (20 ml) was added under argon. The mixture was heated under reflux for 3 h. After addition of diluted HCl, the compound was extracted with diethyl ether from aqueous solution. The ether phase was dried with Na$_2$SO$_4$ and solvent, and some volatile part of residue was distilled. 2′-Diphenylphosphino-2-methoxymethylbiphenyl **6** was recrystallized from ethanol (380 mg, 15%).

The NMR parameters of compound **6** are as follows: ^{31}P NMR (121.49 MHz), δ −13.76; ^{1}H NMR (400 MHz), δ 7,37–7.44 (1H, d, J = 7.70), 7.26–6.92 (16H, m), 6.75–6.72 (1H, d, J = 7.52), 4.02 (2H, s), 3.09 (3H, s). 2′-Diphenylphosphino-2-methoxymethylbiphenyl **6** (380 mg, 0.88 mmol) was dissolved in 10 ml of HBr in glacial acetic acid and heated under reflux for 3 h. The solvent was removed, and the cyclo-o-MitoPh was recrystallized from ethyl acetate/ethanol (290 mg, 93%). The parameters for cyclo-o-MitoPh are as follows: ^{31}P NMR (121.49 MHz), δ 12.68; ^{1}H NMR (300.13 MHz), δ 8.10–8.03 (2H, m), 7.93–7.80 (5H, m), 7.75–7.66 (3H, m), 7.64–7.52 (5H, m), 7.40–7.29 (3H, m); 5.25 (2H, d, J = 14.2); and ^{13}C NMR (300 MHz), δ 149.9 (s), 141.87 (s), 136.2 (d), 135.2 (d), 134.2 (s), 134.0 (s), 133.0 (s), 132.9 (s), 132.8 (s), 132.5 (s), 132.3 (s), 130.7 (s), 130.4 (s), 130.3 (s), 129.6 (s), 128.9 (s), 128.8 (s), 127.8 (s), 127.7 (s), 126.8–126.7 (d), 125.0 (s), 124.9 (s), 116.5 (s), 115.4 (s), 25.7 (s). MS calculated for $C_{25}H_{20}P^+$ was 351.1 and found was 351.1.

HPLC Analyses of the Specific Products Formed from Oxidation of Probes—HPLC-based analyses of the products of oxidation of HE and CBA probes were carried out using Agilent 1100 system equipped with absorption and fluorescence detectors, as described elsewhere (7, 8). Rapid simultaneous monitoring of superoxide and hydrogen peroxide was carried out as reported previously (8), but the Supelco Ascentis Express phenyl-hexyl column (5 cm × 4.6 mm, 2.7 μm) was used. The compounds were eluted isocratically using mobile phase consisting of water (65%), acetonitrile (35%), and trifluoroacetic acid (0.1%) at a flow rate of 2 ml/min. The column temperature was set at 30 °C. Under these conditions the following probes and products were monitored: HE (0.30 min), 2-OH-E$^+$ (0.60 min), E$^+$ (0.67 min), E$^+$-E$^+$ (1.30 min), CBA (0.35 min), and COH (0.42 min). This method was also used in the rapid quantitative analyses of 2-OH-E$^+$ or COH formation from HE or CBA in RAW 264.7 cells generating $O_2^{\bar{\ }}$ or ONOO$^-$.

LC-MS/MS Analyses of o-MitoPhB(OH)$_2$-derived Products—Analyses of o-MitoPhB(OH)$_2$ and its oxidation/nitration products were performed as described recently (21, 32). The method was modified for newly characterized products, including cyclo-o-MitoPh, and deuterated analogs were used as internal standards for quantitative analyses.

Dose-Response Analyses—For determination of the apparent IC$_{50}$ values, the dose-response fitting application was used, as implemented in OriginPro 9.1.0 program (OriginLab Corp.). Equation 2 used for the fitting is as follows:

$$y = A_1 + \frac{A_2 - A_1}{1 + 10^{(\log IC_{50} - \log c)p}} \qquad \text{(Eq. 2)}$$

where y is the measured quantity (proportional to Nox2 enzyme activity); A_1 and A_2 correspond to bottom and top asymptotes, p to the Hill slope, and c is the concentration of the compound.

Results

Overview of HTS/ROS Assays Used in the Identification of Nox Inhibitors—To reliably identify inhibitors of Nox isoforms, we developed the following primary and secondary assays for HTS/ROS analysis (Fig. 2), as described recently (8). Hydropro-
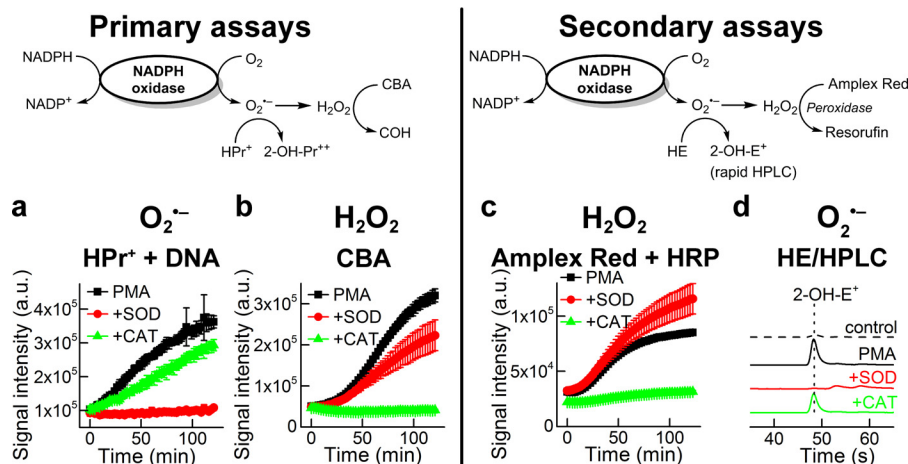
FIGURE 2. **Detection of superoxide and hydrogen peroxide generated from Nox2.** Primary and secondary assays are shown. *a,* increase in fluorescence intensity due to formation of the superoxide-specific product, 2-OH-Pr^{2+}, in *d*HL60 cells activated by PMA. *b,* increase in fluorescence intensity due to catalase-sensitive H$_2$O$_2$ oxidation product, COH, in *d*HL60 cells and PMA. *c,* increase in fluorescence intensity due to formation of resorufin. *d,* HPLC of 2-OH-E$^+$, the specific product of HE and O$_2^-$, in control and PMA-activated *d*HL60 cells in the presence of SOD and catalase (adapted from Ref. 8).

TABLE 2

Step-by-step protocol applied to screen the library of bioactive compounds at The Broad Institute

| |
|---|
| **(i) Cell culture and differentiation of HL60 cells** |
| 1) Grow HL60 cells in RMPI 1640 medium containing 10% FBS and antibiotics |
| 2) To a new flask add HL60 cells (10^5 cells/ml) and add all-*trans*-retinoic acid (final concentration, 1 μM) |
| 3) Incubate the cells for 4 days |
| **(ii) Preparation of cell suspension** |
| 1) Transfer cell suspension into centrifuge tubes and spin down the cells |
| 2) Remove the medium (supernatant) and resuspend the cells in HBSS containing 25 mM HEPES buffer (pH 7.4) and 0.1 mM dtpa |
| 3) Count the cells and prepare the cell suspension in HBSS containing 25 mM HEPES buffer (pH 7.4) and 0.1 mM dtpa at a density of 10^5 cells/ml |
| **(iii) Cell inhibition** |
| 1) Aliquot the cell suspension into black 384-well plates using Thermo Multidrop Combi instrument under sterile conditions |
| 2) Add 100 nl of compound solutions (5–10 mM in DMSO) using a CyBi®-Well (CyBio) equipped with a 100-nl pin tool |
| 3) Incubate the cells with inhibitors for 30 min at 37 °C in a CO$_2$-free incubator |
| **(iv) Plate reader-based 384-well plate-based assays** |
| 1) Add 10 μl/well probes (5× solutions in HBSS containing 25 mM HEPES buffer (pH 7.4), 0.1 mM dtpa, and 0.1 mg/ml BSA) to the 384-well plates containing cells with inhibitors using a Thermo Multidrop Combi instrument. From this point minimize the exposure of plates to light |
| 2) Add 10 μl/well PMA (5× solutions in HBSS containing 25 mM HEPES buffer (pH 7.4), 0.1 mM dtpa and 0.1 mg/ml BSA) to the 384-well plates containing cells with compounds and probes using another Thermo Multidrop Combi instrument |
| 3) Incubate the activated cells with probes for 90 min at 37 °C in a CO$_2$-free incubator |
| 4) Read the fluorescence intensity in the 384-well plates using an Envision (PerkinElmer Life Sciences) plate reader |

pidine (HPr$^+$) was used as a primary probe for extracellular O$_2^-$ measurement (19). HPr$^+$ reacts with O$_2^-$ ($k = 1.2 \times 10^4$ M^{-1} s^{-1}) to form a specific and diagnostic marker product, 2-hydroxypropidium (2-OH-Pr^{2+}) (19). 2-OH-Pr^{2+} fluorescence quantum yield is enhanced >10-fold in the presence of added DNA. Coumarin-7-boronic acid (CBA) was used as another primary assay probe for measuring H$_2$O$_2$. CBA reacts with H$_2$O$_2$ (catalase-sensitive) considerably slower ($k = 1.5$ M^{-1}s^{-1}), as compared with its catalase-insensitive reaction with ONOO$^-$ ($k = 1.1 \times 10^6$ M^{-1} s^{-1}), to form a highly fluorescent product, COH (33). Over the duration of the reaction between CBA and H$_2$O$_2$, there was significantly less spontaneous decomposition of CBA as compared with other boronate probes (33, 34).

The addition of PMA (activator of PKC signaling pathway) to differentiated HL60 cells (overexpressing Nox2) in the presence of HPr$^+$ and DNA causes a linear increase in 2-OH-Pr^{2+} fluorescence (O$_2^-$ reaction) that was inhibited by SOD and not by catalase (Fig. 2). Concomitantly, there is an increase in COH fluorescence (H$_2$O$_2$ reaction with CBA) that is inhibited by catalase and not by SOD (Fig. 2).

In the secondary assay, we used the probe hydroethidine (HE) and detected 2-hydroxyethidium (2-OH-E$^+$) (specific product of HE reaction with O$_2^-$) using ultra-HPLC (Fig. 2). For measuring H$_2$O$_2$, the probe Amplex Red was used in the presence of HRP to monitor resorufin (formed from Amplex Red oxidation with H$_2$O$_2$/HRP) using a plate reader. The addition of PMA to differentiated HL60 cells in the presence of Amplex Red and HRP causes an increase in the fluorescence intensity of resorufin that is abrogated by catalase but not by SOD (Fig. 2). Under these conditions, O$_2^-$ is detected by measuring 2-OH-E$^+$ (by HPLC) that was inhibited by SOD and not by catalase (Fig. 2). These assays provide the foundation for rigorous measurements of O$_2^-$ and H$_2$O$_2$ using three different probes for high throughput screening studies (8).
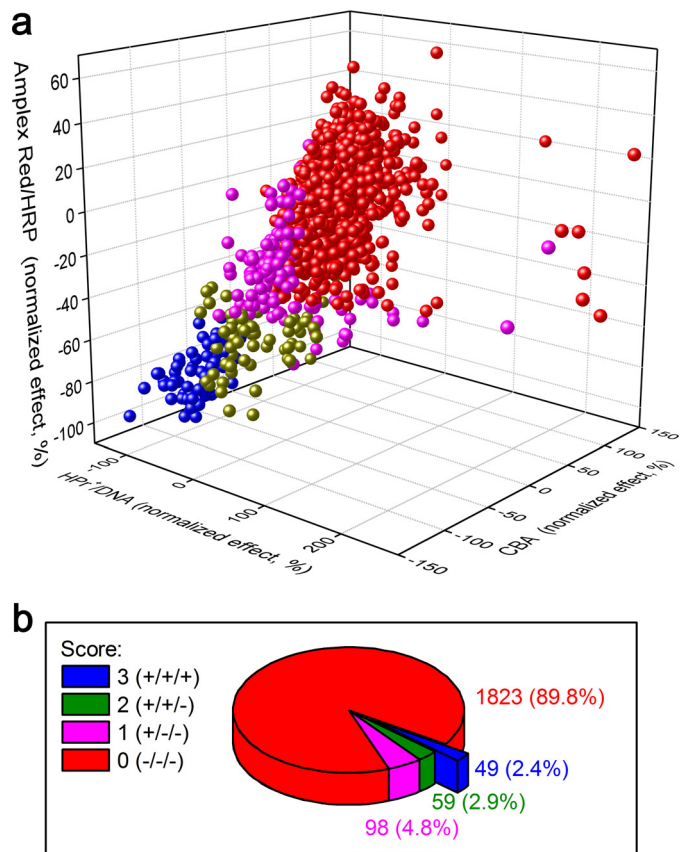
Screening the Library of Bioactive Compounds, Identification of Potential Nox2 Inhibitors—We applied the ROS/HTS assays, as discussed above, to screen a subset library of bioactive drugs as Nox2 inhibitors at Broad Institute Probe Development Center. First, we fulfilled the HTS assay "readiness" criteria for the primary and secondary assay probes (HPr$^+$, CBA, and Amplex Red).
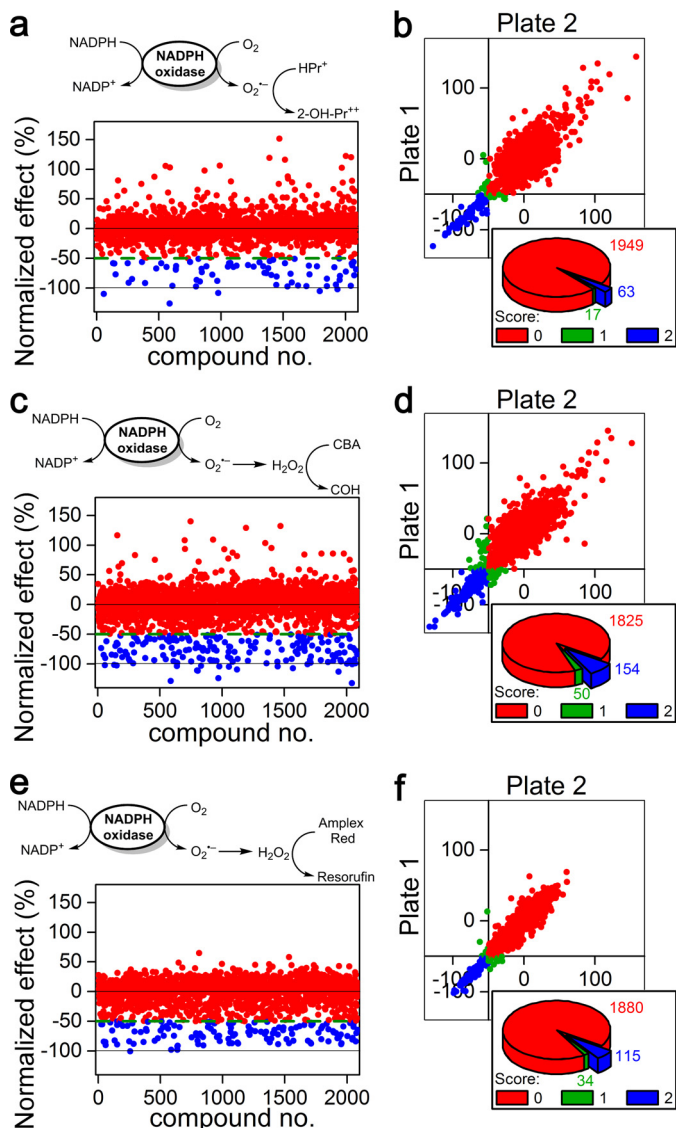
FIGURE 3. **Results of screening of a library of bioactive compounds (≈ 2,000) using the following three probes: hydropropidine (50 μM) in the presence of DNA (0. 1 mg/ml) as a probe for $O_2^{\bar{}}$ (*a* and *b*), and coumarin boronic acid (100 μM, *c* and *d*) or Amplex Red (50 μM) in the presence of HRP (0.1 units/ml, *e* and *f*) as probes for H_2O_2.** *d*HL60 cells were stimulated with PMA (1 μM) to induce Nox2 activity in HBSS supplemented with HEPES buffer (25 mM) and dtpa, 0.1 mM. *a, c,* and *e,* schemes of oxidation of the probes and the results of screening after normalization. *b, d,* and *f,* plate-to-plate reproducibility data and number of negative/inconclusive/positive hits for each assay. Score *0* (*red color*) corresponds to negative; *1* (*green color*) to inconclusive, and *2* (*blue color*) to positive hits.

The list of 2,029 compounds, together with the results of screening of their normalized effects on Nox2 activity using HPr$^+$, CBA, and Amplex Red probes, are shown in supplemental Table 1. The stepwise protocol used in the HTS/ROS studies at Broad Institute is shown in Table 2. The effects of 2,029 compounds on $O_2^{\bar{}}$ formation by monitoring the formation of 2-OH-Pr^{2+} in PMA-activated differentiated HL60 cells are shown in Fig. 3. 2-OH-Pr^{2+} formation in the presence of DMSO and phenylarsine oxide (1 μM) was normalized to 0% (no effect) and −100% (complete inhibition) (Fig. 3a). We set a 50% inhibition (Fig. 3a, *green dashed line*) as a threshold criterion for a "hit." *Blue dots* in Fig. 3a indicate compounds inhib-

FIGURE 4. **Results of screening of a library of bioactive compounds (≈2,000) using the following three probes: hydropropidine (50 μM) in the presence of DNA (0. 1 mg/ml) as a probe for $O_2^{\bar{}}$, and coumarin boronic acid (100 μM) or Amplex Red (50 μM) in the presence of HRP (0.1 units/ml) as probes for H_2O_2.** *a,* correlation of the results of the three assays for Nox2 activity. *b,* results of screening as a percentage of positive hits in one, two, or all three assays. All experimental conditions are as described in Fig. 3.

iting 2-OH-Pr^{2+} formation by >50%, and *red dots* indicate compounds exhibiting <50% inhibition (Fig. 3a). Fig. 3b shows the plate-to-plate comparison showing the reproducibility of data for each compound, and the *pie chart* (*inset* in Fig. 3b) shows 63 out of 2,029 compounds exhibit >50% inhibition of 2-OH-Pr^{2+} formation (*blue chart* with positive >50% inhibition in both plates). Fig. 3, *c* and *d,* shows similar results for COH formation from CBA. One hundred fifty four compounds from the screened library inhibited COH formation by >50% in both plates (Fig. 3d, *inset*). Corresponding results obtained using the Amplex Red probe measuring H_2O_2 are shown in Fig. 3, *e* and *f.*

The three-dimensional hit correlation plot for all three assay probes, HPr$^+$, CBA, and Amplex Red, is shown in Fig. 4a. Of the 2,029 compounds tested, 49 compounds (2.4%, *blue pie chart* in Fig. 4b) were identified as hits with all three probes (Table 3), using 50% inhibition threshold. The *red color* in Fig. 4b corresponds to negative result for all three probes (−/−/−); *magenta* is used for compounds that scored a positive result for a single probe (+/−/−); *green* is used for compounds that scored positively with two probes (+/+/−); and *blue* is used for positive results for all three probes (+/+/+). The list of "positive hits" shown in *blue* in Fig. 4b, together with the average extent of inhibition at ~30 μM concentration is shown (Table

TABLE 3

Positive hits obtained during screening of the library of bioactive compounds using three probes as follows: hydropropidine (50 μM) in the presence of DNA (0.1 mg/ml) as a probe for O_2^-, and coumarin boronic acid (100 μM) or Amplex Red (50 μM) in the presence of HRP (0.1 units/ml) as probes for H_2O_2

Differentiated HL60 cells were stimulated with PMA (1 μM) to induce Nox2 activity in HBSS supplemented with HEPES buffer (25 mM) and dtpa (0.1 mM).

No.	Compound name	HPr$^+$ + DNA	CBA	Amplex Red + HRP
		Normalized score		
1	Miconazole nitrate	−125.8	−128.7	−97.9
2	Methiothepin maleate[a]	−109.5	−101.8	−84.8
3	Mitoxantrone·HCl[a]	−108.1	−104.0	−83.1
4	NNC 55-0396·2HCl	−105.2	−93.9	−80.2
5	Nonoxynol-9	−101.7	−112.9	−77.2
6	5-Nonyloxytryptamine oxalate	−97.0	−111.0	−82.9
7	10-DEBC·HCl[a]	−96.8	−100.4	−82.6
8	Thioridazine·HCl	−96.4	−94.9	−74.2
9	GW7647	−96.2	−132.0	−80.6
10	Diphenyleneiodonium chloride	−95.6	−73.6	−58.4
11	nTZDpa	−94.7	−96.3	−72.1
12	Cetylpyridinium chloride	−93.9	−82.9	−78.3
13	Suloctidil	−91.2	−94.5	−100.3
14	Lylamine·HCl	−90.5	−107.4	−82.8
15	Perphenazine	−88.8	−102.8	−74.1
16	RS 39604·HCl	−88.1	−123.7	−74.1
17	Trifluoperazine·HCl	−86.4	−94.4	−88.6
18	NNC 26-9100	−86.1	−111.4	−88.3
19	Gambogic acid	−84.7	−98.8	−87.8
20	Ginkgolic acid	−84.0	−77.8	−63.4
21	Fluphenazine·HCl	−80.4	−104.1	−88.6
22	Chlorpromazine	−79.7	−95.8	−86.9
23	Amsacrine	−78.8	−99.1	−83.8
24	Amiodarone·HCl	−77.5	−94.3	−67.7
25	SNAP 5089	−76.9	−102.4	−88.8
26	Benzethonium chloride	−76.9	−97.7	−87.3
27	Thimerosal	−76.1	−91.3	−71.2
28	GR 127935·HCl	−73.3	−77.5	−90.6
29	Hexachlorophene	−68.3	−83.6	−64.5
30	Benzbromarone	−67.3	−92.1	−76.4
31	Embelin[a]	−65.0	−87.3	−69.4
32	CGP 71683·HCl	−64.7	−79.8	−71.9
33	Tamoxifen citrate	−63.9	−73.6	−66.6
34	Demethylasterriquinone B1[a]	−63.7	−104.4	−86.9
35	RS 17053·HCl	−63.4	−75.6	−69.1
36	IKK 16	−63.2	−77.9	−59.7
37	Mefloquine	−62.7	−98.5	−90.8
38	GW 3965·HCl	−62.4	−91.7	−87.4
39	Dyclonine·HCl	−62.4	−92.9	−85.7
40	Thiothixene[a]	−61.9	−73.0	−52.6
41	Chlorprothixene·HCl[a]	−58.4	−94.3	−80.2
42	Sulconazole nitrate	−58.2	−71.3	−60.0
43	Trimipramine maleate	−57.9	−101.5	−82.4
44	Tioconazole	−57.9	−91.6	−83.8
45	Trimeprazine tartrate[a]	−56.2	−67.2	−84.8
46	A-7·HCl	−56.1	−95.9	−76.8
47	Mibefradil·2HCl	−51.0	−89.3	−70.5
48	Triflupromazine·HCl	−50.9	−79.0	−60.1
49	L655240[a]	−50.2	−93.3	−72.1

[a] These were identified as pan assay interference compound (38).

3). This list contains Food and Drug Administration-approved drugs that include dopamine receptor blockers and drugs used in the treatment of schizophrenia and antimalarial and antifungal agents. Some of these drugs have been previously used or identified as inhibitors of Nox isoforms (35, 36). Interestingly, the compound, mitoxantrone, identified as the most potent inhibitor of Nox2 activity in dHL60 cells (Table 2) strongly inhibited pancreatic ductal adenocarcinoma survival (37). The positive hits were further evaluated to filter out pan assay interference compounds (38, 39). Of the 49 hits, nine were tested positive when screened against the library of the pan assay interference compounds, as defined in Ref. 38 and shown in Table 3.

Confirmatory Assays, Dose Response, and Oxygen Consumption Measurements—We confirmed the inhibitory effect of compounds selected from positive hits (Table 3) on Nox2 activity by determining their dose response. We screened over 20 commercially available compounds selected from Table 3 for the confirmatory assays. The apparent IC_{50} values for inhibition of Nox2 activity in the dHL60 model determined with a fluorescence plate reader using the CBA-based assay are shown in Table 4. Next, the effect of selected compounds on Nox2 activity was tested by HPLC-based simultaneous monitoring of O_2^- and H_2O_2 (Fig. 5, a and b), by measuring oxygen consumption stimulated by Nox2 activation using the 96-well plate-based extracellular flux analyzer (Seahorse XF96, Fig. 5, c and d) and by monitoring the inhibitory effect on spin-trapped superoxide adduct using DEPMPO (data not shown). Fig. 5a shows the results of the confirmatory assays for selected compounds, sulconazole, mefloquine, cetylpyridinium cation, and DPI, on formation of 2-hydroxyethidium, the specific marker product for O_2^-. Similarly, Fig. 5b shows the effect of these compounds

TABLE 4

IC_{50} values for selected positive hits, determined by monitoring the effect of the compounds on the rate of oxidation of coumarin boronic acid (100 μM) as a probe for H_2O_2

Differentiated HL60 cells were stimulated with PMA (1 μM) to induce Nox2 activity in HBSS supplemented with HEPES buffer (25 mM) and dtpa (0.1 mM) and the extent of probe oxidation was monitored in 384-well plates using fluorescence plate reader.

| No. | Compound | IC_{50} (μM) | |
		Mean	S.D.
1	Amiodarone·HCl	11	2
2	Amoxapine	16	4
3	Benzbromarone	13	1.5
4	Benzethonium chloride	23	0.7
5	Cetylpyridinium chloride	2.3	0.3
6	Chlorpromazine·HCl	13	0.6
7	Clotrimazole	59	25
8	Diphenyleneiodonium	0.08	0.07
9	Dyclonine	39	16
10	Econazole nitrate	22	1.1
11	Hexachlorophene	2.2	0.4
12	Mefloquine·HCl	16	0.4
13	Miconazole	15	6.5
14	Mitoxantrone	18	12
15	Phenylarsine oxide	0.2	0.04
16	Promazine·HCl	31	1.6
17	Sulconazole nitrate	19	2.6
18	Suloctidil	7.7	3.5
19	Tamoxifen citrate	18	0.5
20	Thimerosal	2.2	0.6
21	Thioridazine	9.3	2.1
22	Tioconazole	9.2	0
23	Trifluoperazine	9	2.2
24	Triflupromazine·HCl	12	2.6

on COH, the product of the reaction of CBA probe with H_2O_2. The IC_{50} values for these compounds to inhibit O_2^- and H_2O_2 production also compare favorably with those measured using Nox2-mediated oxygen consumption. We next verified that at these concentrations sulconazole, mefloquine, and cetylpyridinium cations inhibited formation of the DEPMPO-superoxide adduct. All three compounds completely blocked formation of DEPMPO-$^{\cdot}$OOH adduct, when used at 100 μM for sulconazole and mefloquine or 10 μM for cetylpyridinium and DPI cations (data not shown).

Inhibition of Nox2 in Activated RAW 264.7 Macrophages—Following the experiments on dHL60 cells, we tested whether the selected hits can also inhibit Nox2 activity in a different cellular model for Nox2 activity, namely PMA-stimulated RAW 264.7 cells. Activation of RAW 264.7 cells in the presence of the hydroethidine probe led to a significant increase in the HPLC peak of 2-hydroxyethidium (monitored with a fluorescence detector) (Fig. 6a), as reported earlier (7). We measured the yield of 2-OH-E^+ upon PMA-induced Nox2 activation in the presence of several compounds identified as apparent Nox2 inhibitors in dHL60 cells, with DPI used as a positive control for Nox2 inhibition. At these concentrations, all of the compounds tested decreased the intensity of the peak of 2-OH-E^+ (Fig. 6a, fluorescence mode), confirming the ability of these compounds to inhibit Nox2 activity in intact cells. Quantitative analysis of the HPLC data (Fig. 6b) based on the use of authentic standards for 2-OH-E^+, E^+, and E^+-E^+ shows that the compounds inhibit the yield of 2-OH-E^+, while having no effect on ethidium (E^+), the nonspecific oxidation product (with the exception of benzethonium cation), and variable effects on the one-electron oxidation dimeric product (diethidium, E^+-E^+). These results confirm that the HTS hits for Nox2 identified using the differ-

entiated HL60 cells also inhibit O_2^- formation from Nox2 in RAW 264.7 cells.

Do Nox2 Inhibitors Also Inhibit Generation of Peroxynitrite?—Next, we tested whether the compounds listed in Table 4 that inhibit Nox2 activity in PMA-stimulated RAW 264.7 cells could also inhibit generation of peroxynitrite formed from O_2^- and $^{\cdot}$NO reaction in the same cellular model. RAW macrophages were stimulated to co-generate both $^{\cdot}$NO and O_2^- via activation of inducible NOS and Nox2 (using LPS, interferon-γ, and phorbol ester), as reported earlier (7). CBA was used to monitor $ONOO^-$ in cell-free systems and from activated macrophages by monitoring COH (catalase-insensitive) generation (7, 20, 33). Results show that several but not all Nox2 inhibitors identified from the screen of the bioactive library using the dHL60 model inhibited $ONOO^-$-dependent COH formed from CBA. Of note, the compounds inhibiting $ONOO^-$ formation in RAW 264.7 cells also inhibited Nox2 activity in these cells, as demonstrated in Fig. 6. Fig. 7b shows the dose-dependent inhibition of $ONOO^-$ formed from activated macrophages in the presence of selected hits for Nox2 inhibition (*e.g.* DPI, sulconazole, mefloquine, and cetylpyridinium). As shown, DPI potently inhibits $ONOO^-$ formation with an IC_{50} of 0.4 μM. However, DPI being a non-selective inhibitor of flavoproteins may also block $^{\cdot}$NO production by inhibition of inducible NOS. The IC_{50} values for sulconazole, mefloquine and cetylpyridinium cation to inhibit $ONOO^-$ formation were determined to be 33, 36, and 4 μM, respectively. These values compare favorably with their IC_{50} values to inhibit O_2^- generation in PMA-stimulated RAW 264.7 cells (Fig. 7a) and the dHL60 Nox2 model (Table 4). These results suggest that the HTS/ROS assay with CBA can be used to identify novel inhibitors of $ONOO^-$ formation as well.

Specific Detection of a Cyclized Product during Peroxynitrite Reaction with Ortho-substituted Mitophenylboronic Acid—Recently, we developed a new probe, o-MitoPhB(OH)$_2$, that rapidly reacts with $ONOO^-$ forming a minor product, o-MitoPhNO$_2$, that is very specific for $ONOO^-$ (Fig. 8a) and is unaffected by glutathione or other biologically relevant reductants (21, 22). As this product is not fluorescent, we used HPLC with absorption detection for quantitative analyses, and we confirmed it is formed in RAW 264.7 cells in activated macrophages (22). However, using an LC-MS/MS method, we found that this product (*i.e.* o-MitoPhNO$_2$) was detected in a relatively low yield (21). Quantitative analysis of the LC-MS data revealed an additional minor product (m/z = 351) formed during the reaction between o-MitoPhB(OH)$_2$ and $ONOO^-$. The same product was detected in extracts from RAW 264.7 cells, when activated to produce $ONOO^-$ (see below). The structure of this product was assigned to cyclo-o-MitoPh (Fig. 8a, shown in *red*) formed by radical-induced intramolecular cyclization mechanism (Fig. 8a, minor radical pathway). This was supported by the observation that during the reaction of $ONOO^-$ with d_{15}-o-MitoPhB(OH)$_2$ (with all protons on triphenylphosphonium moiety substituted by deuterium), the product with m/z = 365 atomic mass units is formed, indicating the loss of one deuterium atom. The identity of this product was further verified by independent synthesis of cyclo-o-MitoPh (Fig. 9a), and the structure was confirmed by mass spectrometry, NMR, and
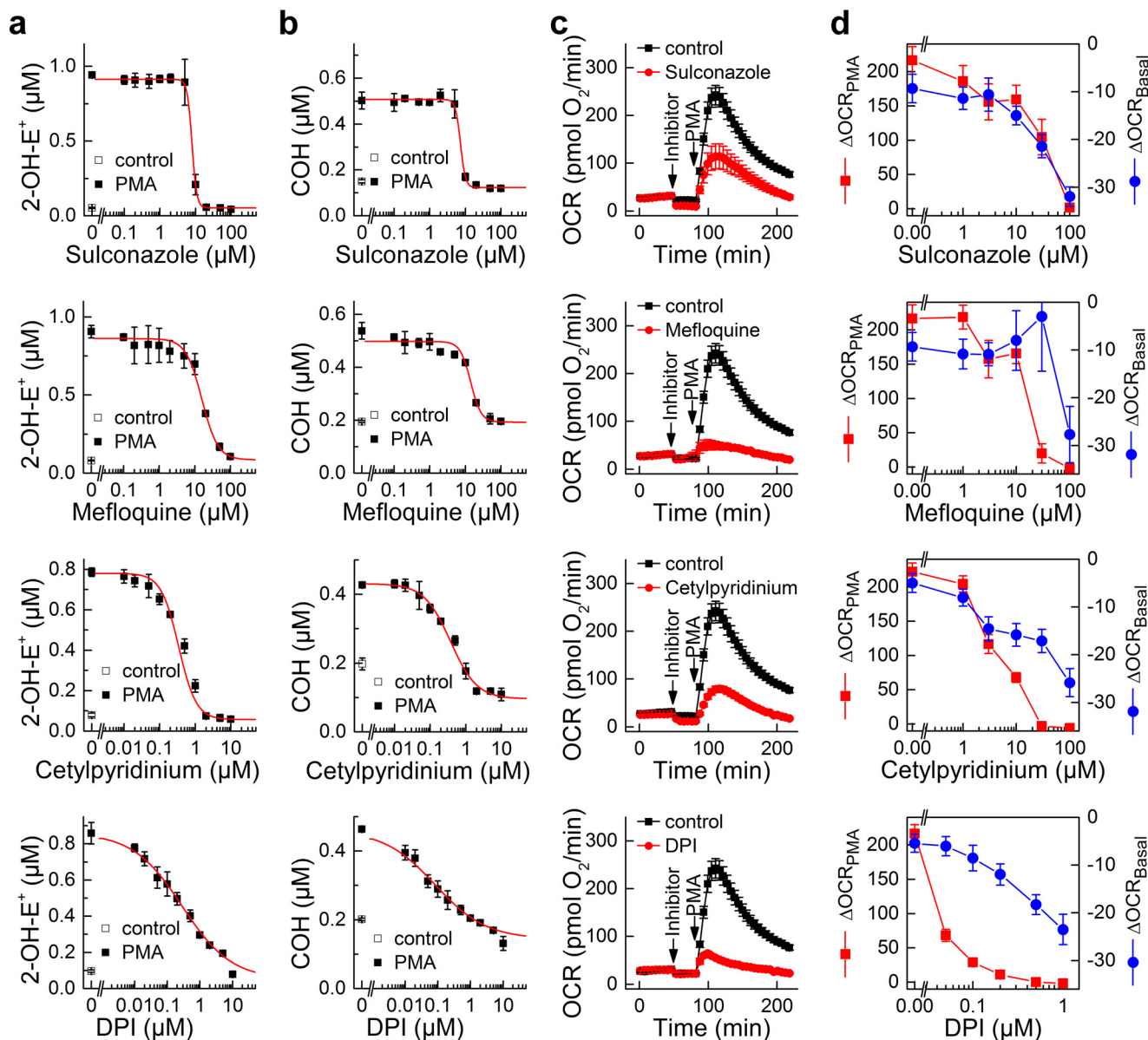
FIGURE 5. **Results of confirmatory assays for selected positive hits from Nox2 inhibitor screening.** Dose-response results of four selected inhibitors of Nox2 on 2-OH-E$^+$ (*a*) and COH (*b*) formation in PMA-activated *d*HL60 cells, using the HPLC-based assay for simultaneous monitoring of O$_2^-$ and H$_2$O$_2$. *c*, effect of the same four inhibitors on oxygen consumption (mitochondrial respiration and NADPH oxidase activation) measured using the Seahorse extracellular flux analyzer. Concentrations of inhibitors are as follows: DPI, 0.1 μ*M*; sulconazole, 30 μ*M*; mefloquine, 30 μ*M*; cetylpyridinium chloride, 10 μ*M*. *d*, dose-dependent response to the same four inhibitors on basal mitochondrial respiration (Δ*OCR*$_{Basal}$, shown in *blue*) and the NADPH oxidase activation by PMA injection (Δ*OCR*$_{PMA}$, shown in *red*).

x-ray crystallography (Fig. 9*b*). The LC-MS/MS parameters (retention time, *m/z* value, and MS/MS fragmentation pattern) of the minor product of *o*-MitoPhB(OH)$_2$ reaction with authentic ONOO$^-$ were identical to those of the authentic cyclo-*o*-MitoPh (Fig. 8, *a* and *c*). The specificity of this product was tested using other oxidants (H$_2$O$_2$ and HOCl), which are known to oxidize boronic compounds and comparing the product identities and distribution (Fig. 8, *b* and *c*). Consistently with our previous research on the chemical reactivity of boronic compounds (20, 32, 40), the reaction between *o*-MitoPhB(OH)$_2$ and H$_2$O$_2$ yielded a single phenolic product (*o*-MitoPhOH), although additional minor products were detected with HOCl and ONOO$^-$. In addition to cyclized (cyclo-*o*-MitoPh) and nitrated (*o*-MitoPhNO$_2$) products, the

products of nitration of *o*-MitoPhOH were also formed in the presence of excess ONOO$^-$. These products showed up at the *m/z* value of 414 and were assigned to isomers of *o*-MitoPh(NO$_2$)OH (Fig. 8*a*) (22). In addition, a small amount of the protonated form of triphenylphosphonium oxide (TPP=O, *m/z* = 279) was also detected. With HOCl, the minor product observed (using excess of HOCl) is chlorinated phenol *o*-MitoPh(Cl)OH (Fig. 8*a*), showing up as a double peak attributed to two isomers. Interestingly, other oxidation products, including triphenylphosphine oxide and brominated phenolic product (*o*-MitoPh(Br)OH)were also formed (Fig. 8). Although triphenylphosphine oxide formation can be explained by a nucleophilic attack of ClO$^-$ on the phosphorus atom of the triphenylphosphonium moiety, the
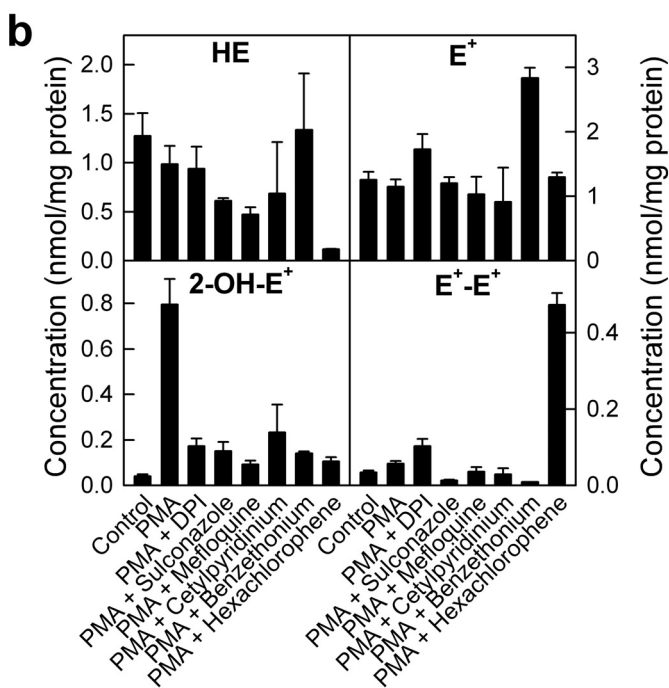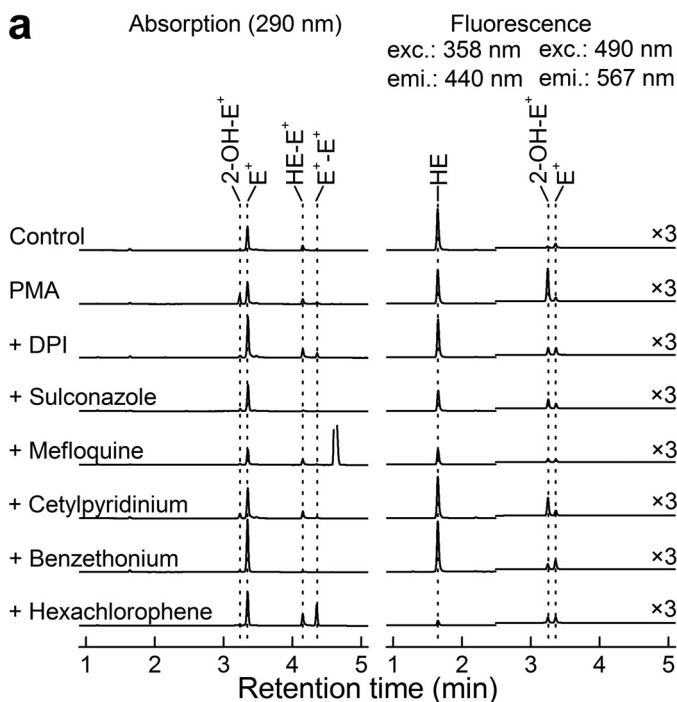
FIGURE 6. **Effect of selected hits on HE oxidation profiles in PMA-stimulated RAW 264.7 macrophages.** *a,* HPLCs at 290 nm (absorption detector) and the HPLC fluorescence traces (excitation/emission wavelengths, as shown). *b,* quantitative analyses of intracellular levels of HE and its oxidation products, after normalization to protein level. Concentrations of agents are as follows: PMA, 1 μM; DPI, 1 μM; sulconazole, 100 μM; mefloquine, 100 μM; cetylpyridinium chloride, 10 μM; benzethonium chloride, 100 μM; hexachlorophene, 100 μM.

brominated phenolic product indicates formation of HOBr via oxidation of the bromide anion (present as a counterion of *o*-MitoPhB(OH)$_2$ probe) by HOCl (41, 42). To test whether *o*-MitoPhB(OH)$_2$ can distinguish between peroxynitrite and myeloperoxidase (MPO)-mediated oxidation/nitration, we determined the products formed by MPO

in the presence of hydrogen peroxide, with or without nitrite (Fig. 10*a*). The results indicate that both cyclo-*o*-MitoPh and *o*-MitoPhNO$_2$ products are specific for ONOO$^-$, although MPO in the presence of nitrite leads to nitration of the phenolic product, formed from oxidation of *o*-MitoPhB(OH)$_2$ by H$_2$O$_2$. The quantitative analysis of the oxidation/nitration of *o*-MitoPhB(OH)$_2$ by ONOO$^-$ indicates that yields of the minor specific products, cyclo-*o*-MitoPh and *o*-MitoPhNO$_2$, are 10.5 $\pm$ 0.5 and 0.5 $\pm$ 0.1%, respectively (Fig. 10*b*). In the case of MPO-mediated oxidation in the presence of sodium nitrite, the major product seems to be nitrated phenols (*o*-MitoPh(NO$_2$)OH). The other product detected was triphenylphosphine oxide, formed by the MPO/H$_2$O$_2$ system both in the absence and presence of nitrite (data not shown). Next, we investigated the formation of peroxynitrite-specific products in activated macrophages and the effect of selected Nox2 inhibitors on the reaction products of *o*-MitoPhB(OH)$_2$ and ONOO$^-$ (Fig. 11). We have shown previously that stimulation of RAW 264.7 cells leads to formation of *o*-MitoPhOH and small amounts of *o*-MitoPhNO$_2$ (21, 22). As shown in Fig. 11, the most exclusive minor product detected in cells was the cyclized product cyclo-*o*-MitoPh. In fact, the amount of *o*-MitoPhNO$_2$ formed in cells is less than 5% of the yield of cyclo-*o*-MitoPh (Fig. 11*c*). The analysis of the effect of inhibitors on the yield of the major phenolic oxidation product of *o*-MitoPhB(OH)$_2$ gives mixed results, with mefloquine actually increasing the yield of this product. This suggests the possibility of multiple pathways of the formation and/or metabolism of the phenolic product inside the cells. In contrast, results show that selected candidate Nox2 inhibitors, including cetylpyridinium, sulconazole, mefloquine, and DPI, inhibit formation of cyclo-*o*-MitoPh and *o*-MitoPhNO$_2$, the diagnostic products for ONOO$^-$ (Fig. 11*c*). This is consistent with the results of measurements of extracellular ONOO$^-$ (Fig. 7*b*) and further demonstrates the added value of determining the specific minor product(s) for ONOO$^-$ reaction with *o*-MitoPhB(OH)$_2$.

Discussion

Significance of Nox Inhibition—Nox enzyme-derived ROS/RNS are now recognized to play a central role in both inflammatory and fibrotic diseases (1, 2). The former includes both classical inflammatory conditions (*e.g.* arthritis and inflammatory bowel disease) and nonclassical conditions in which inflammation plays a central pathogenic role. For example, inflammatory lung diseases include acute respiratory distress syndrome, asthma, and chronic obstructive pulmonary disease, although other inflammatory conditions include Alzheimer and Parkinson diseases, ischemic stroke, and organ reperfusion injury during transplantation (43). Fibrotic diseases include liver fibrosis (*e.g.* following viral infection), idiopathic pulmonary fibrosis, and diabetic kidney disease. Nox2 has been implicated in inflammatory diseases and Nox4 in fibrotic diseases (1, 2). Existing therapies for both classes of diseases include steroids and other anti-inflammatory approaches, but they have proven to be ineffective. Therefore, there is a need for developing novel anti-inflammatory and antifibrotic agents based on other molecular targets. Nox enzymes are especially promising
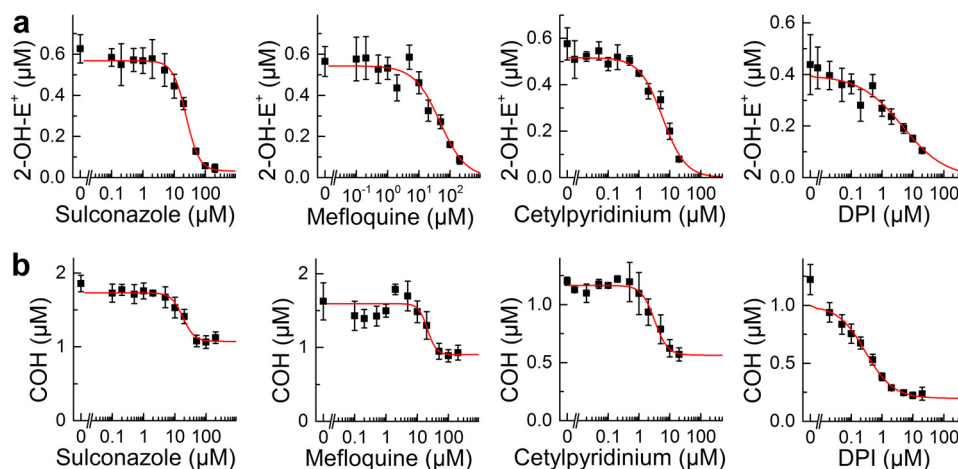
FIGURE 7. **Inhibition of O_2^- and $ONOO^-$ formation from activated RAW 264.7 cells by selected positive hits as follows: sulconazole, mefloquine, cetylpyridinium chloride, and DPI.** Cells were treated with inhibitors for 30 min in Dulbecco's PBS containing glucose and pyruvate followed by addition of PMA (1 μM) and the probe and incubated for 1 h at 37 °C. After incubation, the extracellular media were analyzed for 2-OH-E$^+$ or COH levels using a rapid HPLC method. *a*, RAW 264.7 cells were stimulated with PMA (1 μM) in the presence of HE (10 μM). *b*, RAW 264.7 cells were pretreated overnight with LPS (0.5 μg/ml) and IFNγ (50 units/ml) and stimulated with PMA (1 μM) in the presence of CBA (100 μM).

in this regard due to mounting evidence in humans and in other experimental models (44). Peroxynitrite, the product of diffusion-controlled reaction of nitric oxide and superoxide, has been implicated in several inflammatory diseases (15), including neurodegenerative diseases and chemotherapy-induced nephrotoxicity (45). Recent data also suggest the involvement of $ONOO^-$ in traumatic brain injury-induced neurodegeneration via activation of calpain in neurons (46, 47).

It has been proposed that Nox2-derived ROS/RNS from myeloid-derived suppressor cells in the tumor microenvironment are potentially responsible for decreased T cell reactivity and immunosuppressive effects (48). In this regard, small molecular weight compounds that inhibit Nox2 activity could play a vital role in providing additional mechanistic insight on the immune system in tumor microenvironments. The role of Nox/ROS in biology is paradoxical (49). High levels of O_2^- generated from Nox2 are essential for cell killing and host defense, whereas in other cells, low levels of ROS (O_2^- and H_2O_2 or both) generated from Nox are important for cell signaling (*e.g.* NF-κB activation). Nox inhibitors effectively abrogated proliferation of various cancer cell models (50). Preliminary results show that several compounds identified as potential Nox2 inhibitors (Table 4) significantly inhibit proliferation of human pancreatic cancer cells (data not shown). It is likely that follow-up studies will greatly improve the potency and selectivity of hit compounds using medicinal chemistry. Although this study is restricted to the Nox2 isoform, future investigations will broaden the scope of work to include other Nox isoforms using the appropriate HTS-compatible cell lines.

HTS/ROS/RNS Assay—ROS/RNS do not represent a single entity, but encompass a wide range of reactive species that exhibit oxidizing, nitrating, nitrosating, and halogenating properties (51, 52). To better understand the pathophysiological consequences of ROS/RNS, it is crucial to identify and characterize the species that are specifically responsible for a given "biologic and toxicologic" effect and to inhibit the specific sources of ROS/RNS generation (53). Doxorubicin, one of the most widely used chemotherapeutics, causes myocardial

inflammation that is attributed to Nox-induced ROS/RNS formation in inflammatory cells (54–56). Genetic disruption of Nox2 mitigated doxorubicin-mediated contractile dysfunction, oxidative/nitrative stress, and inflammation (56). Thus, selective targeting of Nox2 may provide a novel therapeutic strategy for mitigation of ROS/RNS and cardiotoxic side effects, while maximizing its antitumor efficacy (56). To date, only a limited number of Nox isoform-selective inhibitors are available (57, 58). This is due in part to serious limitations of the existing ROS/RNS assays as described below.

Previous approaches have used sensitive but nonselective and artifact-prone ROS/RNS probes (59) for detecting Nox-derived oxidants, resulting in a high rate of false positives and potentially missing weaker but selective hits lost in the "noise." Many HTS-based H_2O_2 assays to detect Nox inhibitors included the enzyme HRP. The lack of probes' selectivity for specific oxidant and the susceptibility of the HTS assays to peroxidase substrates and inhibitors led to the controversy over the Nox-inhibitory potency of the positive hits selected, including apocynin, VAS2870, and 2-acetylphenothiazine (36, 60, 61). In fact, one of the authors recently reported a new myeloperoxidase inhibitor, identified during the HTS campaign for Nox2 inhibitors, using the L-012 probe as a Nox2 activity reporter (62). Using the present HTS/ROS approach, it is conceivable that false positives will be decreased by >75%, with the assay specificity allowing identification of weaker inhibitors that can later be improved through medicinal chemistry. In this work, we describe the use of ROS/RNS-specific probes whose redox chemistry is better understood with respect to reaction kinetics, stoichiometry and reaction products (63). Selective monitoring of specific ROS in the HTS assay is important. For example, these HTS assays can be extended to other cell types to gain new insight regarding enzymatic sources of ROS generation and subsequently unravel the role of ROS in disease-related biological processes. It is conceivable that a similar HTS/ROS assay may be used to identify inhibitors of other oxidants (*e.g.* hypochlorous acid) and their sources of generation using other fluorescent probes (Table 1).
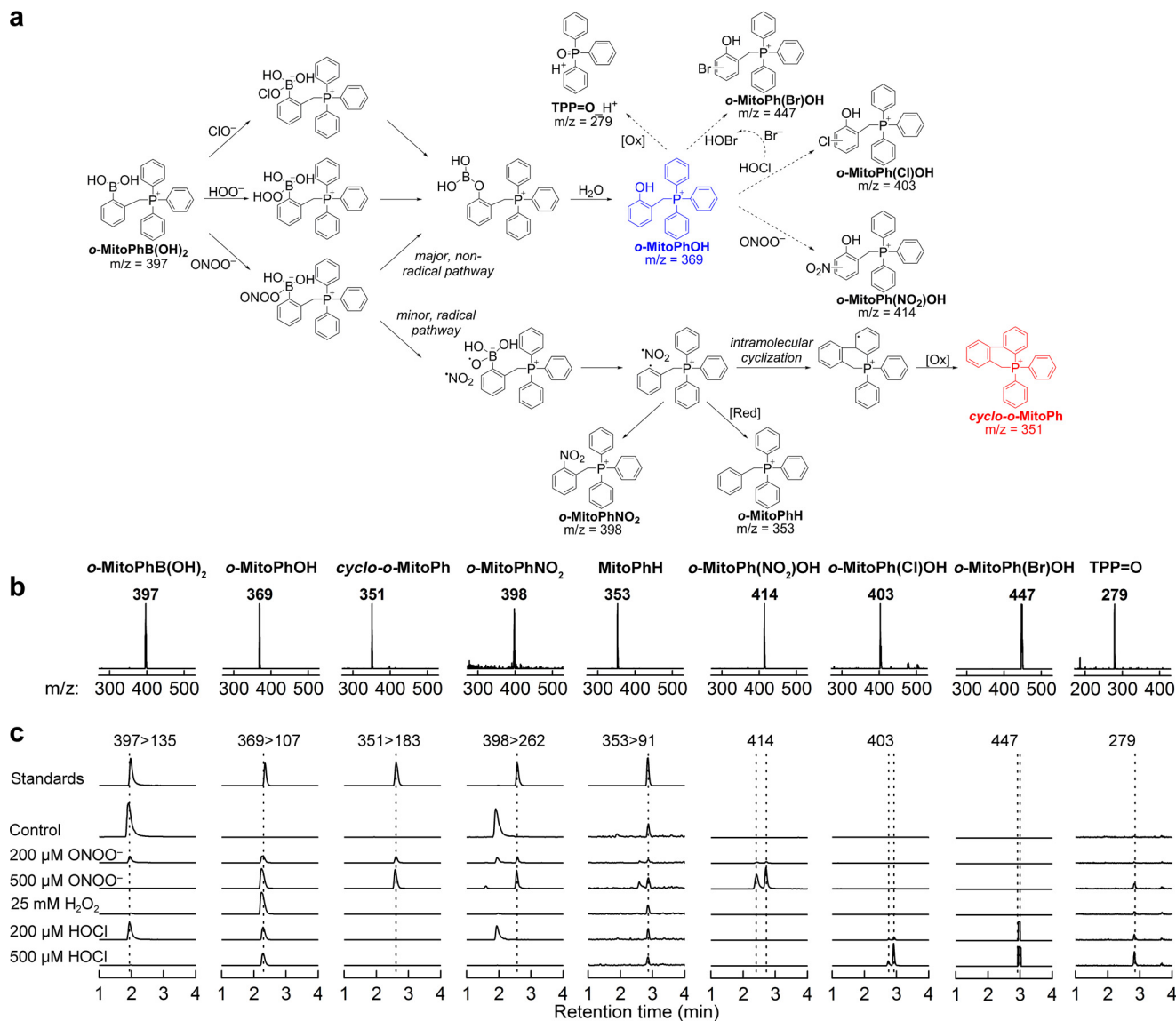
FIGURE 8. **Detection and characterization of specific products from the probe, *o*-MitoPhB(OH)₂.** *a,* proposed mechanism of oxidation of *o*-MitoPhB(OH)₂ by ONOO⁻, H₂O₂, and HOCl. The major oxidation product, common for all oxidants, is shown in *blue,* and the peroxynitrite-specific cyclization product is shown in *red. Dashed arrows* indicate the possible subsequent oxidation/nitration/halogenation reactions of the major product, *o*-MitoPhOH. *b,* mass spectra of the products determined from the on-line spectra of the corresponding LC-MS peaks. *c,* LC-MS/MS traces (multiple reaction monitoring, indicated by parent ion > fragment ion pair) or LC-MS traces (single ion monitoring, indicated by the *m/z* value monitored) of the products detected during the reaction between *o*-MitoPhB(OH)₂ probe and the authentic ONOO⁻, H₂O₂, and HOCl.
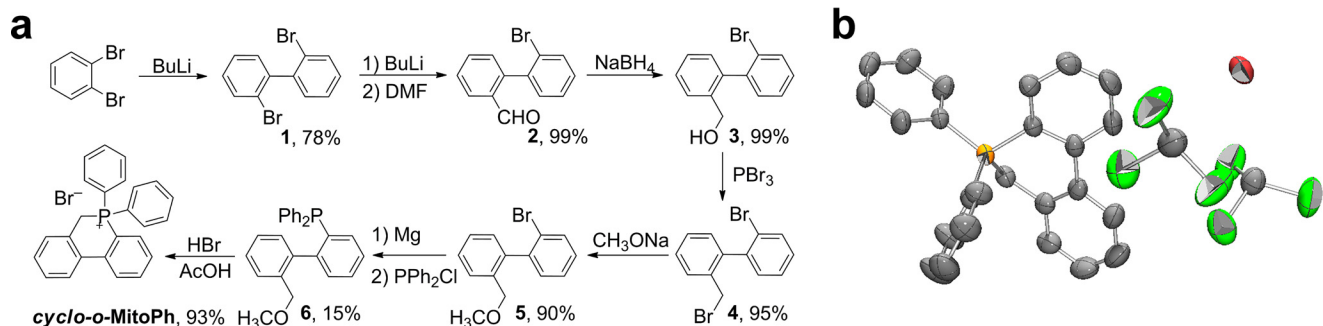
FIGURE 9. **Independent synthetic scheme for cyclo-*o*-MitoPh and structure determination by x-ray diffraction.** *a,* synthesis, and *b,* crystal structure of cyclo-*o*-MitoPh.

In this study, we identified new, oxidant-specific, products of the reaction of *o*-MitoPhB(OH)₂ with ONOO⁻ and HOCl (Fig. 8). In the presence of the excess oxidant, the major phenolic product undergoes nitration or chlorination reaction, respectively, leading to isomeric nitro- or chloro-derivatives of Mito-PhOH. Also, in the presence of HOBr, analogous products (*i.e.*
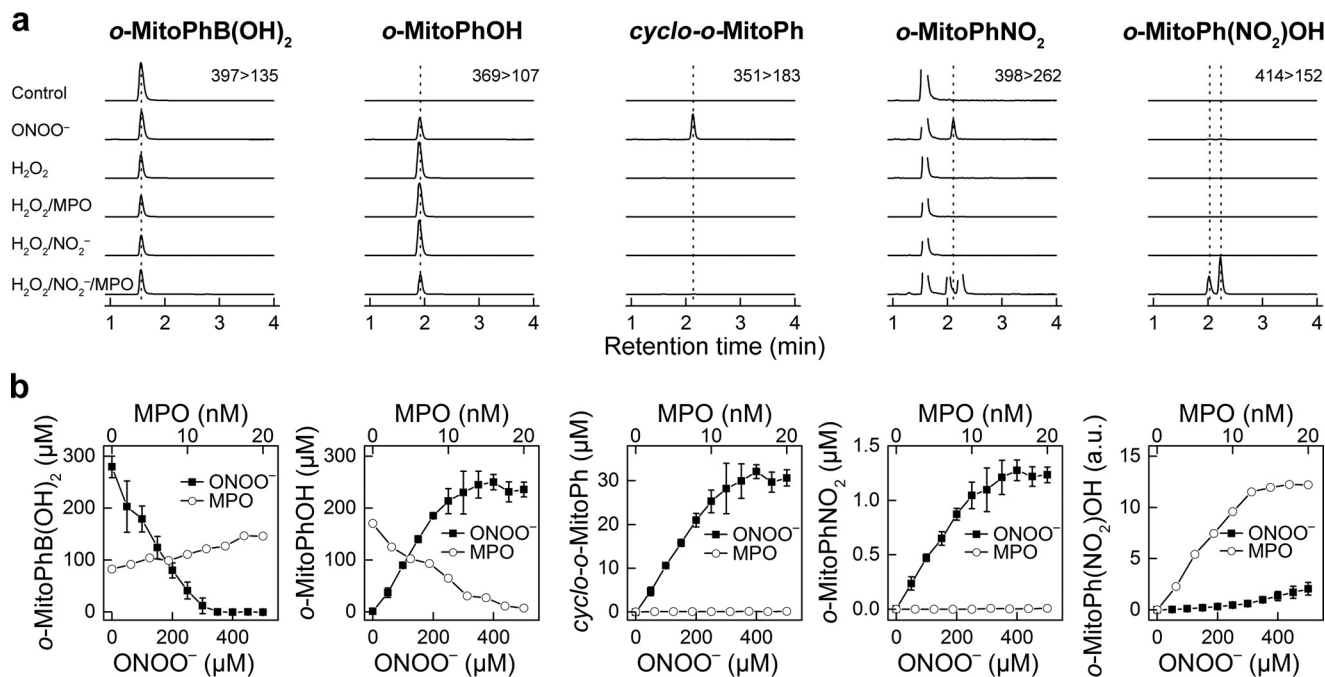
FIGURE 10. **Comparison of the products formed from oxidation of *o*-MitoPhB(OH)$_2$ by peroxynitrite and myeloperoxidase.** *a*, LC-MS/MS traces (multiple reaction monitoring, indicated by parent ion > fragment ion pair) of the products detected during the reaction between *o*-MitoPhB(OH)$_2$ probe (280 μM) and ONOO$^-$ (100 μM), H$_2$O$_2$ (1 mM), H$_2$O$_2$ (1 mM) + MPO (10 nM), H$_2$O$_2$ (1 mM) + NaNO$_2$ (10 mM), and H$_2$O$_2$ (1 mM) + NaNO$_2$ (10 mM) + MPO (10 nM). *b*, results of titration of *o*-MitoPhB(OH)$_2$ (280 μM) with ONOO$^-$ and MPO. *o*-MitoPhB(OH)$_2$ was incubated with MPO in the presence of H$_2$O$_2$ (1 mM) and NaNO$_2$ (10 mM) in 0.1 M phosphate buffer (pH 7.4) for 1 h at 25 °C.

MitoPh(Br)OH) are formed. With excess ONOO$^-$ or HOCl, the triphenylphosphine oxide was also formed (Fig. 8). Interestingly, with peroxynitrite, the most exclusive minor product, cyclo-*o*-MitoPh, was formed even when the probe was present in excess of the oxidant. The lack of effect of biologically relevant reductants (GSH and NADH) and the low efficiency of trapping of the phenyl radical (22) may be explained by rapid intramolecular cyclization due to addition of the phenyl radical to the benzene ring of the triphenylphosphonium moiety (Fig. 8*a*). As this product is not formed with any other oxidant or nitrating agent tested, it can serve as a specific diagnostic product of ONOO$^-$ and should be used as the ultimate proof of peroxynitrite intermediacy.

Inhibitory Mechanism of Nox2 Positive Hits on ROS Formation—Screening of the library of over 2,000 bioactive compounds generated a relatively high amount of positive hits, with the lowest yield (3.1%) using the hydropropidine-based assay. This was expected, as the compounds tested show a variety of biological activities and do not predominantly target NADPH oxidase. However, screening of a large, chemically diverse library of compounds will produce a significantly lower yield of active compounds. The HTS compatibility of the three assays (HPr$^+$, CBA, and Amplex Red-based) and the use of rapid HPLC analyses in the 384-well plate format will enable rapid orthogonal screenings to filter out false positives. Additionally, the use of chemical structure-based filters to remove pan assay interference compounds should further decrease the amount of compounds selected for post-screening studies/hit optimization process.

HL60 cells differentiated into a neutrophil-like phenotype by DMSO or all-*trans*-retinoic acid exhibited high expression of

Nox2 as confirmed by Western blotting of both membrane-bound gp91^{phox} and cytosolic p47^{phox} subunits (8). The differentiated cells were compared with nondifferentiated cells in their response to PMA, an activator of protein kinase C, leading to the phosphorylation of the p47^{phox} cytosolic subunit, which, in turn, binds to p22^{phox} membrane protein. After the assembly of all cytosolic and membrane components, NADPH is oxidized, and its electrons are transferred to oxygen, generating O$_2^-$. Small molecules can inhibit O$_2^-$ and H$_2$O$_2$ by targeting specific steps of Nox activation as follows: Nox expression, ligand receptor binding, trafficking of Nox components to cell membrane, activation and assembly of Nox complex, NADPH binding, and electron transfer from the active site of the enzyme (64). To identify target of inhibition of Nox2, it is essential to perform a comprehensive analysis of phosphorylation of proteins of the regulatory subunits and the effect of inhibitors on phosphorylation and translocation of the cytosolic subunits to the membrane. These aspects will be a part of our future research. Some of the Nox2 inhibitors (*e.g.* promazines) identified in this work have previously been shown to block Nox2 activity in cell-free assays (36). Of added significance is the fact that selected hits also affect basal mitochondrial respiration in *d*HL60 cells (Fig. 5, *c* and *d*). Whereas sulconazole inhibits PMA response (Nox2 activation) and basal respiration similarly, other compounds are more selective in their inhibition of Nox2 activity, with little or less pronounced inhibition of mitochondrial function at selected concentrations. Although the inhibition of basal mitochondrial respiration and Nox2 activity may be linked, the inhibition of mitochondrial respiration *per se* is unlikely to block Nox2 activity. In fact, we have previously shown that rotenone, an inhibitor of mitochondrial complex I,

a

b

c
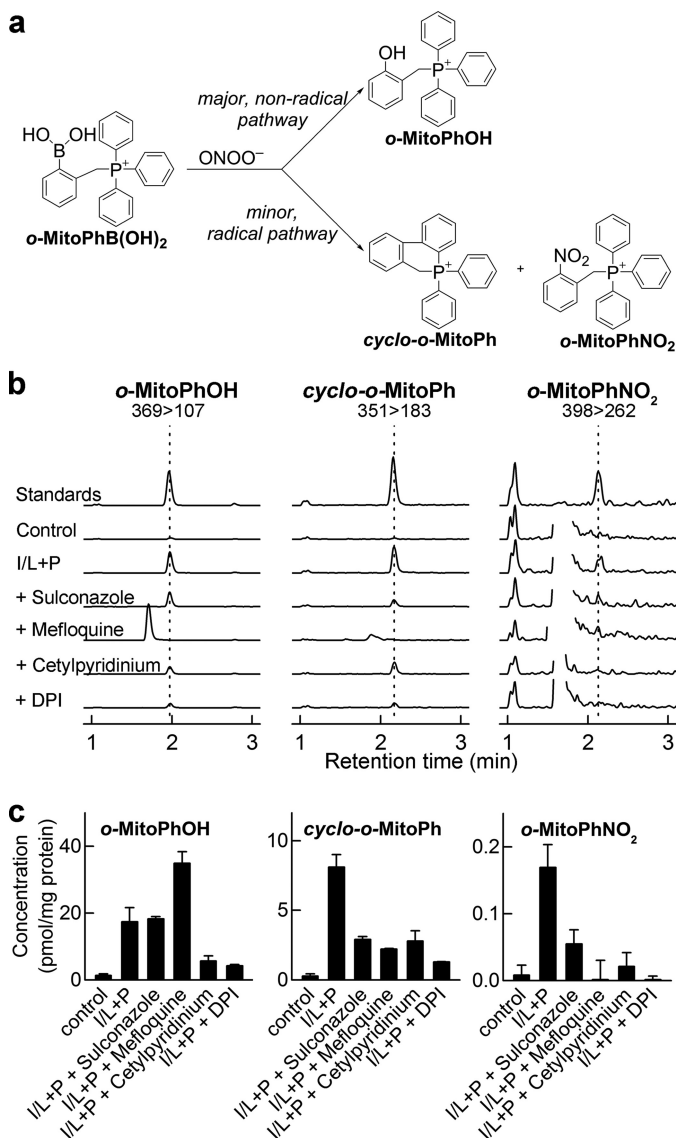
FIGURE 11. **Effect of selected positive hits for Nox2 inhibition on formation of *o*-MitoPhB(OH)₂ oxidation/nitration products, *o*-MitoPhOH, *cyclo*-*o*-MitoPh, and *o*-MitoPhNO₂.** *a,* scheme showing the major and minor products of the reaction of *o*-MitoPhB(OH)₂ and ONOO⁻. *b,* LC-MS/MS traces corresponding to *o*-MitoPhOH, *cyclo*-*o*-MitoPh, and *o*-MitoPhNO₂, recorded during analysis of extracts of RAW 264.7 cells incubated with *o*-MitoPhB(OH)₂. Concentration of standards were as follows: 100 nM (*o*-MitoPhOH), 30 nM (*cyclo*-*o*-MitoPh), and 1 nM (*o*-MitoPhNO₂). *c,* quantitative analysis of the intracellular levels *o*-MitoPhOH, *cyclo*-*o*-MitoPh, and *o*-MitoPhNO₂, detected in cells stimulated to produce ONOO⁻ in the absence or presence of Nox2 inhibitors, as indicated. RAW 264.7 cells were stimulated with IFNγ, LPS, and PMA (shown as *I/L + P*) and incubated for 1 h in the presence of *o*-MitoPhB(OH)₂ (50 μM). Inhibitors were added immediately before addition of PMA and the probe. Concentrations of agents are as follows: LPS, 0.5 μg/ml; IFNγ, 50 units/ml; PMA, 1 μM; DPI, 1 μM; sulconazole, 100 μM; mefloquine, 100 μM; cetylpyridinium chloride, 10 μM.

inhibits basal mitochondrial respiration in *d*HL60 cells, without affecting the Nox2 activity, as measured by the PMA-stimulated increase in the rate of oxygen consumption (8). It is also worth noting that DPI, a non-selective inhibitor of flavoenzymes, inhibits Nox2 activity at a significantly lower concentration (0.1 μM) than required for inhibiting the basal mitochondrial respiration (≈1 μM) (Fig. 5*d*).

The proposed method of high throughput screening of Nox inhibitors in intact cells will likely yield many positive hits that

affect the Nox enzyme indirectly, as discussed above. The detailed mechanistic studies may provide new information on the pathways/factors controlling Nox enzyme activity and yield potentially new inhibitors for clinical trials, based on drug repurposing strategy.

Author Contributions—B. K. conceived and coordinated the study and wrote the paper. J. Z. designed, performed, analyzed, and interpreted the data, prepared the figures, and revised the paper critically. M. Z. performed the experiments and provided the technical assistance. G. C. designed and performed the Seahorse experiments and obtained cell proliferation data. M. H. and M. M. A. synthesized hydropropidine and *cyclo*-*o*-MitoPh product, respectively. O. O. provided assistance in these syntheses and structure analyses. R. P. synthesized *o*-MitoPhB(OH)₂, its oxidation/nitration products and corresponding deuterated analogs. A. S. helped in characterization of minor products of *o*-MitoPhB(OH)₂ oxidation. J. D. L. revised the manuscript for intellectual content. L. V. provided training, assisted in screening of the bioactive libraries at Broad Institute, and performed first pass analysis of the screening results. All authors reviewed the results and approved the final version of the manuscript.

References

1. Bulua, A. C., Simon, A., Maddipati, R., Pelletier, M., Park, H., Kim, K. Y., Sack, M. N., Kastner, D. L., and Siegel, R. M. (2011) Mitochondrial reactive oxygen species promote production of proinflammatory cytokines and are elevated in TNFR1-associated periodic syndrome (TRAPS). *J. Exp. Med.* **208,** 519–533
2. Hecker, L., Cheng, J., and Thannickal, V. J. (2012) Targeting NOX enzymes in pulmonary fibrosis. *Cell. Mol. Life Sci.* **69,** 2365–2371
3. Leto, T. L., Morand, S., Hurt, D., and Ueyama, T. (2009) Targeting and regulation of reactive oxygen species generation by Nox family NADPH oxidases. *Antioxid. Redox Signal.* **11,** 2607–2619
4. Lambeth, J. D. (2004) NOX enzymes and the biology of reactive oxygen. *Nat. Rev. Immunol.* **4,** 181–189
5. Nisimoto, Y., Diebold, B. A., Cosentino-Gomes, D., Constentino-Gomes, D., and Lambeth, J. D. (2014) Nox4: a hydrogen peroxide-generating oxygen sensor. *Biochemistry* **53,** 5111–5120
6. Altenhöfer, S., Radermacher, K. A., Kleikers, P. W., Wingler, K., and Schmidt, H. H. (2015) Evolution of NADPH oxidase inhibitors: selectivity and mechanisms for target engagement. *Antioxid. Redox Signal.* **23,** 406–427
7. Zielonka, J., Zielonka, M., Sikora, A., Adamus, J., Joseph, J., Hardy, M., Ouari, O., Dranka, B. P., and Kalyanaraman, B. (2012) Global profiling of reactive oxygen and nitrogen species in biological systems: high throughput real-time analyses. *J. Biol. Chem.* **287,** 2984–2995
8. Zielonka, J., Cheng, G., Zielonka, M., Ganesh, T., Sun, A., Joseph, J., Michalski, R., O'Brien, W. J., Lambeth, J. D., and Kalyanaraman, B. (2014) High throughput assays for superoxide and hydrogen peroxide: design of a screening workflow to identify inhibitors of NADPH oxidases. *J. Biol. Chem.* **289,** 16176–16189
9. Daiber, A., August, M., Baldus, S., Wendt, M., Oelze, M., Sydow, K., Kleschyov, A. L., and Munzel, T. (2004) Measurement of NAD(P)H oxidase-derived superoxide with the luminol analogue L-012. *Free Radic. Biol. Med.* **36,** 101–111
10. Zielonka, J., Lambeth, J. D., and Kalyanaraman, B. (2013) On the use of L-012, a luminol-based chemiluminescent probe, for detecting superoxide and identifying inhibitors of NADPH oxidase: a reevaluation. *Free Radic. Biol. Med.* **65,** 1310–1314

11. Beckman, J. S., Beckman, T. W., Chen, J., Marshall, P. A., and Freeman, B. A. (1990) Apparent hydroxyl radical production by peroxynitrite: implications for endothelial injury from nitric oxide and superoxide. *Proc. Natl. Acad. Sci. U.S.A.* **87,** 1620–1624

12. Radi, R., Beckman, J. S., Bush, K. M., and Freeman, B. A. (1991) Peroxynitrite oxidation of sulfhydryls. The cytotoxic potential of superoxide and nitric oxide. *J. Biol. Chem.* **266,** 4244–4250

13. Beckman, J. S. (2009) Understanding peroxynitrite biochemistry and its potential for treating human diseases. *Arch. Biochem. Biophys.* **484,** 114–116

14. Al Ghouleh, I., Khoo, N. K., Knaus, U. G., Griendling, K. K., Touyz, R. M., Thannickal, V. J., Barchowsky, A., Nauseef, W. M., Kelley, E. E., Bauer, P. M., Darley-Usmar, V., Shiva, S., Cifuentes-Pagano, E., Freeman, B. A., Gladwin, M. T., and Pagano, P. J. (2011) Oxidases and peroxidases in cardiovascular and lung disease: new concepts in reactive oxygen species signaling. *Free Radic. Biol. Med.* **51,** 1271–1288

15. Pacher, P., Beckman, J. S., and Liaudet, L. (2007) Nitric oxide and peroxynitrite in health and disease. *Physiol. Rev.* **87,** 315–424

16. Ye, Y., Quijano, C., Robinson, K. M., Ricart, K. C., Strayer, A. L., Sahawneh, M. A., Shacka, J. J., Kirk, M., Barnes, S., Accavitti-Loper, M. A., Radi, R., Beckman, J. S., and Estévez, A. G. (2007) Prevention of peroxynitrite-induced apoptosis of motor neurons and PC12 cells by tyrosine-containing peptides. *J. Biol. Chem.* **282,** 6324–6337

17. Guzik, T. J., and Harrison, D. G. (2006) Vascular NADPH oxidases as drug targets for novel antioxidant strategies. *Drug Discov. Today* **11,** 524–533

18. Cifuentes-Pagano, E., Meijles, D. N., and Pagano, P. J. (2014) The quest for selective nox inhibitors and therapeutics: challenges, triumphs and pitfalls. *Antioxid. Redox Signal.* **20,** 2741–2754

19. Michalski, R., Zielonka, J., Hardy, M., Joseph, J., and Kalyanaraman, B. (2013) Hydropropidine: a novel, cell-impermeant fluorogenic probe for detecting extracellular superoxide. *Free Radic. Biol. Med.* **54,** 135–147

20. Zielonka, J., Sikora, A., Hardy, M., Joseph, J., Dranka, B. P., and Kalyanaraman, B. (2012) Boronate probes as diagnostic tools for real time monitoring of peroxynitrite and hydroperoxides. *Chem. Res. Toxicol.* **25,** 1793–1799

21. Zielonka, J., Sikora, A., Adamus, J., and Kalyanaraman, B. (2015) Detection and differentiation between peroxynitrite and hydroperoxides using mitochondria-targeted arylboronic acid. *Methods Mol. Biol.* **1264,** 171–181

22. Sikora, A., Zielonka, J., Adamus, J., Debski, D., Dybala-Defratyka, A., Michalowski, B., Joseph, J., Hartley, R. C., Murphy, M. P., and Kalyanaraman, B. (2013) Reaction between peroxynitrite and triphenylphosphonium-substituted arylboronic acid isomers: identification of diagnostic marker products and biological implications. *Chem. Res. Toxicol.* **26,** 856–867

23. Zhao, H., Joseph, J., Fales, H. M., Sokoloski, E. A., Levine, R. L., Vasquez-Vivar, J., and Kalyanaraman, B. (2005) Detection and characterization of the product of hydroethidine and intracellular superoxide by HPLC and limitations of fluorescence. *Proc. Natl. Acad. Sci. U.S.A.* **102,** 5727–5732

24. Zielonka, J., Vasquez-Vivar, J., and Kalyanaraman, B. (2008) Detection of 2-hydroxyethidium in cellular systems: a unique marker product of superoxide and hydroethidine. *Nat. Protoc.* **3,** 8–21

25. Teufelhofer, O., Weiss, R. M., Parzefall, W., Schulte-Hermann, R., Micksche, M., Berger, W., and Elbling, L. (2003) Promyelocytic HL60 cells express NADPH oxidase and are excellent targets in a rapid spectrophotometric microplate assay for extracellular superoxide. *Toxicol. Sci.* **76,** 376–383

26. Seitz, P. M., Cooper, R., Gatto, G. J., Jr., Ramon, F., Sweitzer, T. D., Johns, D. G., Davenport, E. A., Ames, R. S., and Kallal, L. A. (2010) Development of a high throughput cell-based assay for superoxide production in HL-60 cells. *J. Biomol. Screen.* **15,** 388–397

27. Zhang, J. H., Chung, T. D., and Oldenburg, K. R. (1999) A simple statistical parameter for use in evaluation and validation of high throughput screening assays. *J. Biomol. Screen.* **4,** 67–73

28. Nicholls, D. G., Darley-Usmar, V. M., Wu, M., Jensen, P. B., Rogers, G. W., and Ferrick, D. A. (2010) Bioenergetic profile experiment using C2C12 myoblast cells. *J. Vis. Exp.* **46,** 2511

29. Oba, M., Iida, M., and Nishiyama, K. (2001) Generation and reactions of transient 9-silaphenanthrene derivative. *Organometallics* **20,** 4287–4290

30. Cookson, E. A., and Crofts, P. C. (1966) Phosphorus heterocycles. Part I. A conjugated cyclic methylenephosphorane. *J. Chem. Soc, C,* 2003–2005

31. Goy, R., Apfel, U. P., Elleouet, C., Escudero, D., Elstner, M., Görls, H., Talarmin, J., Schollhammer, P., González, L., and Weigand, W. (2013) A silicon-heteroaromatic system as photosensitizer for light-driven hydrogen production by hydrogenase mimics. *Eur. J. Inorg. Chem.* **2013,** 4466–4472

32. Sikora, A., Zielonka, J., Lopez, M., Dybala-Defratyka, A., Joseph, J., Marcinek, A., and Kalyanaraman, B. (2011) Reaction between peroxynitrite and boronates: EPR spin-trapping, HPLC analyses, and quantum mechanical study of the free radical pathway. *Chem. Res. Toxicol.* **24,** 687–697

33. Zielonka, J., Sikora, A., Joseph, J., and Kalyanaraman, B. (2010) Peroxynitrite is the major species formed from different flux ratios of co-generated nitric oxide and superoxide: direct reaction with boronate-based fluorescent probe. *J. Biol. Chem.* **285,** 14210–14216

34. Van de Bittner, G. C., Dubikovskaya, E. A., Bertozzi, C. R., and Chang, C. J. (2010) *In vivo* imaging of hydrogen peroxide production in a murine tumor model with a chemoselective bioluminescent reporter. *Proc. Natl. Acad. Sci. U.S.A.* **107,** 21316–21321

35. Cohen, H. J., Chovaniec, M. E., and Ellis, S. E. (1980) Chlorpromazine inhibition of granulocyte superoxide production. *Blood* **56,** 23–29

36. Seredenina, T., Chiriano, G., Filippova, A., Nayernia, Z., Mahiout, Z., Fioraso-Cartier, L., Plastre, O., Scapozza, L., Krause, K. H., and Jaquet, V. (2015) A subset of *N*-substituted phenothiazines inhibits NADPH oxidases. *Free Radic. Biol. Med.* **86,** 239–249

37. Burkhart, R. A., Peng, Y., Norris, Z. A., Tholey, R. M., Talbott, V. A., Liang, Q., Ai, Y., Miller, K., Lal, S., Cozzitorto, J. A., Witkiewicz, A. K., Yeo, C. J., Gehrmann, M., Napper, A., Winter, J. M., *et al.* (2013) Mitoxantrone targets human ubiquitin-specific peptidase 11 (USP11) and is a potent inhibitor of pancreatic cancer cell survival. *Mol. Cancer Res.* **11,** 901–911

38. Baell, J. B., and Holloway, G. A. (2010) New substructure filters for removal of pan assay interference compounds (PAINS) from screening libraries and for their exclusion in bioassays. *J. Med. Chem.* **53,** 2719–2740

39. Baell, J., and Walters, M. A. (2014) Chemistry: chemical con artists foil drug discovery. *Nature* **513,** 481–483

40. Sikora, A., Zielonka, J., Lopez, M., Joseph, J., and Kalyanaraman, B. (2009) Direct oxidation of boronates by peroxynitrite: mechanism and implications in fluorescence imaging of peroxynitrite. *Free Radic. Biol. Med.* **47,** 1401–1407

41. Ximenes, V. F., Morgon, N. H., and de Souza, A. R. (2015) Hypobromous acid, a powerful endogenous electrophile: experimental and theoretical studies. *J. Inorg. Biochem.* **146,** 61–68

42. Kumar, K., and Margerum, D. W. (1987) Kinetics and mechanism of general-acid-assisted oxidation of bromide by hypochlorite and hypochlorous acid. *Inorg. Chem.* **26,** 2706–2711

43. Drummond, G. R., Selemidis, S., Griendling, K. K., and Sobey, C. G. (2011) Combating oxidative stress in vascular disease: NADPH oxidases as therapeutic targets. *Nat. Rev. Drug Discov.* **10,** 453–471

44. Jaquet, V., Scapozza, L., Clark, R. A., Krause, K. H., and Lambeth, J. D. (2009) Small-molecule NOX inhibitors: ROS-generating NADPH oxidases as therapeutic targets. *Antioxid. Redox Signal.* **11,** 2535–2552

45. Mukhopadhyay, P., Horváth, B., Zsengellér, Z., Zielonka, J., Tanchian, G., Holovac, E., Kechrid, M., Patel, V., Stillman, I. E., Parikh, S. M., Joseph, J., Kalyanaraman, B., and Pacher, P. (2012) Mitochondrial-targeted antioxidants represent a promising approach for prevention of cisplatin-induced nephropathy. *Free Radic. Biol. Med.* **52,** 497–506

46. Deng, Y., Thompson, B. M., Gao, X., and Hall, E. D. (2007) Temporal relationship of peroxynitrite-induced oxidative damage, calpain-mediated cytoskeletal degradation and neurodegeneration after traumatic brain injury. *Exp. Neurol.* **205,** 154–165

47. Khan, M., Dhammu, T. S., Matsuda, F., Annamalai, B., Dhindsa, T. S., Singh, I., and Singh, A. K. (2016) Targeting the nNOS/peroxynitrite/calpain system to confer neuroprotection and aid functional recovery in a mouse model of TBI. *Brain Res.* **1630,** 159–170

48. Corzo, C. A., Cotter, M. J., Cheng, P., Cheng, F., Kusmartsev, S., Sotomayor, E., Padhya, T., McCaffrey, T. V., McCaffrey, J. C., and Gabrilovich, D. I. (2009) Mechanism regulating reactive oxygen species in tumor-induced myeloid-derived suppressor cells. *J. Immunol.* **182,** 5693–5701

49. Holmström, K. M., and Finkel, T. (2014) Cellular mechanisms and physi-

ological consequences of redox-dependent signalling. *Nat. Rev. Mol. Cell Biol.* **15,** 411–421

50. Bonner, M. Y., and Arbiser, J. L. (2012) Targeting NADPH oxidases for the treatment of cancer and inflammation. *Cell. Mol. Life Sci.* **69,** 2435–2442

51. Winterbourn, C. C. (2008) Reconciling the chemistry and biology of reactive oxygen species. *Nat. Chem. Biol.* **4,** 278–286

52. Kalyanaraman, B. (2013) Teaching the basics of redox biology to medical and graduate students: oxidants, antioxidants and disease mechanisms. *Redox Biol.* **1,** 244–257

53. Murphy, M. P., Holmgren, A., Larsson, N. G., Halliwell, B., Chang, C. J., Kalyanaraman, B., Rhee, S. G., Thornalley, P. J., Partridge, L., Gems, D., Nyström, T., Belousov, V., Schumacker, P. T., and Winterbourn, C. C. (2011) Unraveling the biological roles of reactive oxygen species. *Cell Metab.* **13,** 361–366

54. Bendall, J. K., Cave, A. C., Heymes, C., Gall, N., and Shah, A. M. (2002) Pivotal role of a gp91(phox)-containing NADPH oxidase in angiotensin II-induced cardiac hypertrophy in mice. *Circulation* **105,** 293–296

55. Mukhopadhyay, P., Rajesh, M., Bátkai, S., Kashiwaya, Y., Haskó, G., Liaudet, L., Szabó, C., and Pacher, P. (2009) Role of superoxide, nitric oxide, and peroxynitrite in doxorubicin-induced cell death *in vivo* and *in vitro*. *Am. J. Physiol. Heart Circ. Physiol* **296,** H1466–H1483

56. Zhao, Y., McLaughlin, D., Robinson, E., Harvey, A. P., Hookham, M. B., Shah, A. M., McDermott, B. J., and Grieve, D. J. (2010) Nox2 NADPH oxidase promotes pathologic cardiac remodeling associated with doxorubicin chemotherapy. *Cancer Res.* **70,** 9287–9297

57. Borbély, G., Szabadkai, I., Horváth, Z., Markó, P., Varga, Z., Breza, N., Baska, F., Vántus, T., Huszár, M., Geiszt, M., Hunyady, L., Buday, L., Orfi, L., and Kéri, G. (2010) Small-molecule inhibitors of NADPH oxidase 4. *J. Med. Chem.* **53,** 6758–6762

58. Wind, S., Beuerlein, K., Eucker, T., Müller, H., Scheurer, P., Armitage, M. E., Ho, H., Schmidt, H. H., and Wingler, K. (2010) Comparative pharmacology of chemically distinct NADPH oxidase inhibitors. *Br. J. Pharmacol.* **161,** 885–898

59. Gianni, D., Taulet, N., Zhang, H., DerMardirossian, C., Kister, J., Martinez, L., Roush, W. R., Brown, S. J., Bokoch, G. M., and Rosen, H. (2010) A novel and specific NADPH oxidase-1 (Nox1) small-molecule inhibitor blocks the formation of functional invadopodia in human colon cancer cells. *ACS Chem. Biol.* **5,** 981–993

60. Heumüller, S., Wind, S., Barbosa-Sicard, E., Schmidt, H. H., Busse, R., Schröder, K., and Brandes, R. P. (2008) Apocynin is not an inhibitor of vascular NADPH oxidases but an antioxidant. *Hypertension* **51,** 211–217

61. Hirano, K., Chen, W. S., Chueng, A. L., Dunne, A. A., Seredenina, T., Filippova, A., Ramachandran, S., Bridges, A., Chaudry, L., Pettman, G., Allan, C., Duncan, S., Lee, K. C., Lim, J., Ma, M. T., *et al.* (2015) Discovery of GSK2795039, a novel small molecule NADPH oxidase 2 inhibitor. *Antioxid. Redox Signal.* **23,** 358–374

62. Li, Y., Ganesh, T., Diebold, B. A., Zhu, Y., McCoy, J. W., Smith, S. M., Sun, A., and Lambeth, J. D. (2015) Thioxo-dihydroquinazolin-one compounds as novel inhibitors of myeloperoxidase. *ACS Med. Chem. Lett.* **6,** 1047–1052

63. Kalyanaraman, B., Darley-Usmar, V., Davies, K. J., Dennery, P. A., Forman, H. J., Grisham, M. B., Mann, G. E., Moore, K., Roberts, L. J., 2nd., and Ischiropoulos, H. (2012) Measuring reactive oxygen and nitrogen species with fluorescent probes: challenges and limitations. *Free Radic. Biol. Med.* **52,** 1–6

64. Streeter, J., Thiel, W., Brieger, K., and Miller, F. J., Jr. (2013) Opportunity Nox: the future of NADPH oxidases as therapeutic targets in cardiovascular disease. *Cardiovasc. Ther.* **31,** 125–137